JCTC Journal of Chemical Theory and Computation

Article

pubs.acs.org/JCTC

Quantum Chemical Benchmarking, Validation, and Prediction of Acidity Constants for Substituted Pyridinium Ions and Pyridinyl Radicals

John A. Keith[†] and Emily A. Carter*[,†,‡]

[†]Department of Mechanical and Aerospace Engineering, [‡]Program in Applied and Computational Mathematics, and the Andlinger Center for Energy and the Environment, Princeton University, Princeton, New Jersey 08544-5263, United States

Supporting Information

ABSTRACT: Sensibly modeling (photo)electrocatalytic reactions involving proton and electron transfer with computational quantum chemistry requires accurate descriptions of protonated, deprotonated, and radical species in solution. Procedures to do this are generally nontrivial, especially in cases that involve radical anions that are unstable in the gas phase. Recently, pyridinium and the corresponding reduced neutral radical have been postulated as key catalysts in the reduction of CO_2 to methanol. To assess practical methodologies to describe the acid/base chemistry of these species, we employed density functional theory (DFT) in tandem with implicit solvation models to calculate acidity constants for 22 substituted pyridinium cations and their corresponding pyridinyl radicals in water solvent. We first benchmarked our calculations against experimental pyridinium deprotonation energies in both gas and aqueous phases. DFT with hybrid exchange-correlation functionals provide chemical accuracy for gas-phase data and allow absolute prediction of experimental pK_as with unsigned errors under 1 pK_a unit. The accuracy of this economical pK_a calculation approach was further verified by benchmarking against highly accurate (but very expensive) CCSD(T)-F12 calculations. We compare the relative importance and sensitivity of these energies to selection of solvation model, solvation energy definitions, implicit solvation cavity definition, basis sets, electron densities, model geometries, and mixed implicit/explicit models. After determining the most accurate model to reproduce experimentally-known pK_as from first principles, we apply the same approach to predict pK_as for radical pyridinyl species that have been proposed relevant under electrochemical conditions. This work provides considerable insight into the pitfalls using continuum solvation models, particularly when used for radical species.

INTRODUCTION

One of the greatest challenges facing science and engineering in the 21st century is finding ways to fulfill our demands for energy with sustainable energy sources.[1−3] Experts anticipate no single source will completely replace fossil fuels as presently used, though solar energy shoulders high expectations to satisfy a large portion of future global demand. Besides photovoltaics,[4−6] which directly convert sunlight into electricity, photoelectrocatalysis is a promising direction to make highly endoergic, fuel-producing chemical reactions (e.g., water splitting[7−9] or CO_2 reduction[10−12]) economically and efficiently powered by sunlight.

When used correctly, quantum chemistry can elucidate reaction mechanisms to better engineer catalysts. Unfortunately, computational modeling of photoelectrocatalysis is still nascent due to its multifaceted complexity. In electrocatalysis, external potentials promote reaction intermediates (e.g., combinations of ions and radicals) into roles not normally played under vacuum or even in solution-phase environments. Rationally designing catalysts to manipulate those species is crucial. One should then efficiently and consistently model electronic structures of molecules in their neutral, ionic (e.g., protonated), and/or radical forms. Determining strategies to predict the acidities of both closed-shell and radical species would be a large step toward characterizing (photo)-electrocatalysis through computation.

Quantum chemistry, particularly density functional theory (DFT) coupled with implicit solvation models,[13−15] is used ubiquitously to study homogeneous and heterogeneous reaction mechanisms.[16−25] Similar approaches involving DFT and other post-Hartree−Fock (HF) *ab initio* methods have been used to understand acid/base chemistry in chemically and biologically relevant systems.[26−50] These works show that several standard techniques reproduce solvation trends quite well, but predicting quantitatively accurate acidity constants (i.e., pK_as) is challenging since errors of 1.4 kcal/mol in calculated aqueous-phase deprotonation energies lead to errors of 1 pK_a unit. Each component of the thermochemical cycle used to determine aqueous-phase deprotonation energies must be accurate. Minimizing errors usually requires a combination of better treatment of electronic correlation with higher-level post-HF energies, more robust implicit solvation models, or careful bookkeeping of energies so that errors cancel as much as possible. Ho and Coote dedicatedly summarized many years of accumulated technical details and issues associated with first principles pK_a calculations;[51,52] here we extend those works to discuss issues pertaining to radical acidities.

We report a comprehensive benchmarking of acidities of substituted pyridinium molecules, a molecular class with a sizable experimental reference data set available. This data set

Received: April 10, 2012
Published: August 7, 2012

dx.doi.org/10.1021/ct300295g | J. Chem. Theory Comput. 2012, 8, 3187−3206

contains gas-phase proton affinities (the negative of deprotonation enthalpies) and gas-phase basicities (the negative of deprotonation free energies) as well as aqueous-phase acid dissociation constants for nonradical species. This work has far-reaching contexts since pyridine plays many versatile roles in chemistry. It is used in industry as a solvent and as a precursor for pharmaceuticals.[53] Pyridine was recently found to unexpectedly participate in vanadium-mediated alcohol oxidation mechanisms,[54] and substituted pyridine molecules are models for nicotinamide adenine dinucleotide (NAD) compounds, which are ubiquitously present in cellular metabolic processes.[55] Raman spectroscopy, neutron scattering, molecular dynamics, and quantum chemical studies have characterized the nature of water interactions with pyridine.[56−59] Small angle neutron scattering experiments on methyl-substituted pyridines (i.e., picolines) have indicated that methyl groups near the N-terminus create differentiable degrees of local hydrophobicity.[60] Finally, there is also interest in how radical pyridinyl species participate in atmospheric[61] and photoelectrochemical reactions.[62,63]

Regarding the latter phenomenon, Bocarsly and co-workers recently employed a photoelectrochemical cell using a p-type GaP semiconductor electrode and a pyridinium catalyst to selectively convert CO_2 into methanol.[64] Intriguingly, this process operates with very high faradaic yields at *underpotentials*. Experimental efforts to determine the mechanism of this process have been ongoing; however, mechanistic understanding for this and other processes would be enhanced if theory could elucidate its complex electrochemistry. It has been postulated that H^+/CO_2 exchange at pyridinyl radicals, proposed to form by one-electron reduction of pyridinium ions, is the key step in forming a species capable of reducing CO_2.[65,66] Although we have recently shown that one-electron reductions to form pyridinyls will be highly endoergic,[67] our focus here is on identifying reliable calculation schemes to determine acid−base properties of the reduced species, i.e., pyridinyl pK_as.

Many researchers have reported pK_as for smaller sets of substituted pyridinium cations with a variety of different schemes and computational approaches.[26,29,31,42,68−70] Acidities of various radicals in solution have been obtained before with quantum chemistry calculations.[71−81] Pyridinyl acidities present an additional degree of complexity since pyridine radical anions have *negative* electron affinities,[82] and therefore extreme care is required to properly characterize their physically-relevant electronic states.[83,84] Acidity constants of pyridinyl molecules can be obtained from effective 'titrations' that measure the pH dependence of transient absorption spectra. However, most of these experimental pyridinyl studies are related to NAD/NADH$^+$,[85−87] which have strongly electron-withdrawing carbonyl substituents that (as we later show) can greatly influence the acidity of the pyridine group. In the mid 1970s, Neta noted that electron spin resonance spectra for several substituted pyridinyls were unchanged across a pH range from 7.0−14, meaning that their pK_as must be above 14.[88,89] To the best of our knowledge, no theoretical work has explicitly addressed the acidities of radical pyridinyls. We do so here.

Acid Dissociation Constants from First Principles. Brønsted-Lowry acidity (or basicity) is a measure of how readily the molecule donates (or accepts) a proton in solution. Acidity (or basicity) constants for deprotonation reactions are related to the Gibbs free energy change upon proton transfer. Weak bases ionize water to form conjugate acids, and pyridine itself is a weak base due to the N atom's lone pair that accepts protons from solution. Therefore, the acidities of protonated cations (such as pyridinium, eq 1) are often of interest in acid/base chemistry.

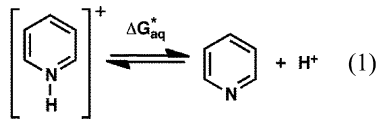

(1)

Calculating acidity constants from quantum chemistry calculations (see refs 51 and 52 for additional details) merely requires using eq 2 after the aqueous-phase free energy of deprotonation is obtained. The latter is derived using a thermodynamically consistent cycle, such as that shown in Scheme 1.

$$pK_a = -\log K_a = \frac{\Delta G^*_{aq}(I)}{2.303 \cdot RT} \quad (2)$$

Scheme 1. Thermodynamic Cycle to Compute the pK_as for a Conjugate Acid, BH$^+$, Requiring the Solvation Energy of a Proton

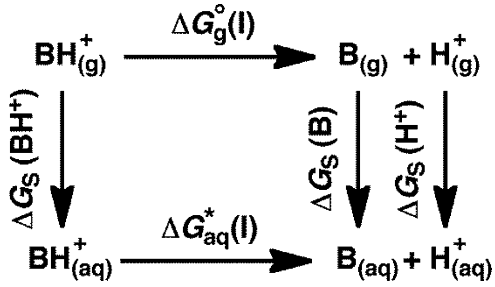

The horizontal arrows in Scheme 1 involve gas-phase reactions (the '°' denotes a standard state at 1 atm, i.e., with a molar volume of 24.46 L) and aqueous-phase reactions (the '*' denotes the aqueous-phase standard states with a molar volume of 1 L). The vertical arrows denote the total free energies to transfer individual species from gas phase into a solvent. Within Scheme 1, the aqueous-phase reaction free energy (ΔG^*_{aq}) requires taking the gas-phase reaction energy (ΔG°_g) plus the ΔG_S values of the products minus the ΔG_S of the reactant. The ΔG_S values contain not only free energies due to solvation but also additional energy contributions due to standard state changes as well as energies resulting from how the solvation energies are calculated (eq 3).

$$\Delta G_S \approx \Delta G^*_S + \Delta G^{\circ\rightarrow *} + \Delta G^{*\rightarrow \mathrm{conc.}} + \Delta E_{\mathrm{aq\text{-}gas}} \quad (3)$$

Following Ben-Naim and Marcus,[90,91] the free energy of solvation, ΔG^*_S, is defined as the work due to placing a solute into a solvent at a fixed standard state (e.g., 1 M). Solvation energies are conventionally denoted with the '*' since aqueous solutions have a 1-M standard state. Semiempirical continuum solvation models have been developed to give reasonably accurate ΔG^*_S values;[13−15,92] however, users of these models are usually left responsible to include the other energy terms in eq 3.

Transferring a solute molecule from gas phase into solvent phase also involves moving from a 1-atm standard state into the 1-M standard state (see left-hand side of Scheme 2). Thus, an additional energy contribution, typically denoted as $\Delta G^{\circ\rightarrow *}$ (see eq 4), should be included.

Scheme 2. Free Energy Schematic Showing Relative Energy Differences between Gas Phase and Solvated Species at Different Standard States

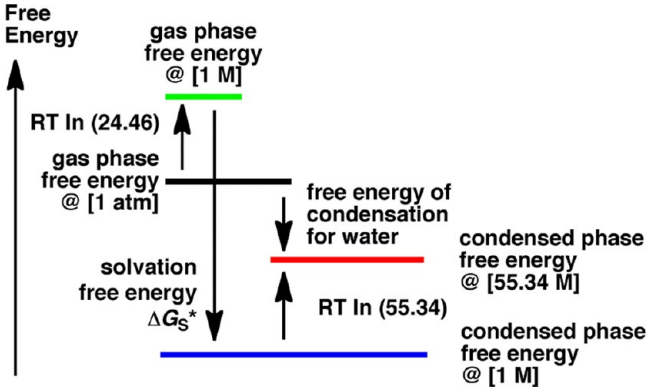

$$\Delta G^{o\rightarrow *} = -T\Delta S^{o\rightarrow *} = -RT\ln\left(\frac{V^*}{V^o}\right)(\text{at constant } P \text{ and } T) = -RT\ln\left(\frac{1\text{ L}}{24.46\text{ L}}\right) = RT\ln(24.46) = 1.89\text{ kcal/mol } (T = 298\text{ K}) \quad (4)$$

Similar energy contributions must also be included if solvated molecules reside in a different standard state than 1 M, e.g., water molecules solvated by water, which has a standard state concentration of 55.34 M. Scheme 2 depicts how the solvation free energy of a water molecule, ΔG_S^*, in liquid water can be obtained by taking the free energy of condensation (i.e., the free energy to go from gaseous water at 1 atm to 55.34 M liquid water, −2.05 kcal/mol) minus the $\Delta G^{o\rightarrow *}$ value needed for the transfer from 1 atm → 1 M (eq 4) minus the free energy to transfer from 1 M → 55.34 M ($\Delta G^{*\rightarrow conc.}$, eq 5) resulting in −2.05 − 1.89 − 2.38 = −6.31 kcal/mol.

$$\Delta G^{*\rightarrow conc.} = -T\Delta S^{*\rightarrow conc.} = -RT\ln\left(\frac{V^{conc.}}{V^*}\right)(\text{at constant } P \text{ and } T) = -RT\ln\left(\frac{(1/55.34)\text{ L}}{1\text{ L}}\right) = RT\ln(55.34) = 2.38\text{ kcal/mol } (T = 298\text{ K}) \quad (5)$$

ΔG_S^* values are calculated from a solvation calculation at a fixed geometry, usually from a gas-phase geometry optimization. In molecules where electronic polarization is strong enough to significantly alter a molecular geometry (e.g., zwitterions or other species that undergo charge transfer), ΔG_S^* is better obtained from a molecular geometry optimized under the influence of the solvation model. If gas-phase geometries are used, eq 3 (for solutes at a 1-M standard state) reduces to $\Delta G_S = \Delta G_S^* + \Delta G^{o\rightarrow *}$. If solvent-optimized geometries are used, eq 3 must include the additional term $\Delta E_{aq\text{-}gas}$ that accounts for the electronic energy difference between the solvent-optimized and gas-phase-optimized geometries in order to close the thermochemical cycle. This term is usually negligible unless the geometry optimization with the continuum model leads to a structure with different H-bonding and/or electrostatic interactions than that from the gas-phase geometry optimization.

Depending on the implicit solvation model used, solvation energies may sometimes improve when adding explicit solvent molecules to the solvation calculation,[34,39,93−100] particularly when the molecule is charged, solvated in water, and has a functional group capable of forming strong H-bonds. Typically, the largest improvements occur with small ions that consist of only a few atoms, since highly localized charge can delocalize into the surrounding solvent, causing the implicit solvation model to operate on an unphysical charge density.[39] Molecules with an accessible electron lone pair such as pyridine may also benefit by including explicit water molecules near H-bonding sites. Adding explicit waters to a solvation model is not trivial, however, and doing so in a stepwise manner requires a thermodynamically consistent explicit/implicit cluster model.[44,100,101] In this approach, each of the ΔG_S energies for each species in Scheme 1 do not come directly from eq 3 but from a separate thermodynamic cycle for each charged (or uncharged) species, $X^{m\pm}$ (Scheme 3).

Regardless if gas-phase or solvent-phase geometries are used, Scheme 3 assumes $\Delta G_{aq}^* = 0$ for converting an aqueous-phase $X_{(aq)}^{m\pm}$ and an aqueous-phase water cluster, $(H_2O)_{n(aq)}$, into an aqueous-phase $[X(H_2O)_n]_{(aq)}^{m\pm}$ cluster. This conditionality makes $\Delta G_S(X^{m\pm})$ solvable via the gas-phase clustering energy to build the waters around $X_{(g)}^{m\pm}$ to form $[X(H_2O)_n]_{(g)}^{m\pm}$, $\Delta G_g^o(\text{bind})$, plus the $\Delta G_S([X(H_2O)_n]^{m\pm})$ value (obtained from eq 3) minus the $\Delta G_S((H_2O)_n)$ value (obtained from eq 3 or from its own thermochemical cycle as done in ref 27). Recall that each ΔG_S term contains an identical $\Delta G^{o\rightarrow *}$ value. Since there is one more reactant than product in this cycle, a net $\Delta G^{o\rightarrow *}$ term appears in the computation of $\Delta G_S(X^{m\pm})$. $\Delta G_S((H_2O)_n)$ requires additional care to treat because it consists of a water cluster entering liquid water with a standard state of 55.34 M. Recall adding one water molecule into water results in $\Delta G^{*\rightarrow conc.} = RT\ln(55.34) = +2.38$ kcal/mol (eq 5). Adding a water cluster $(H_2O)_n$ into water results in $\Delta G^{*\rightarrow conc.}$

Scheme 3. Thermodynamic Cycle to Compute ΔG_S for a General Species within a Mixed Implicit-Explicit Solvation Approach

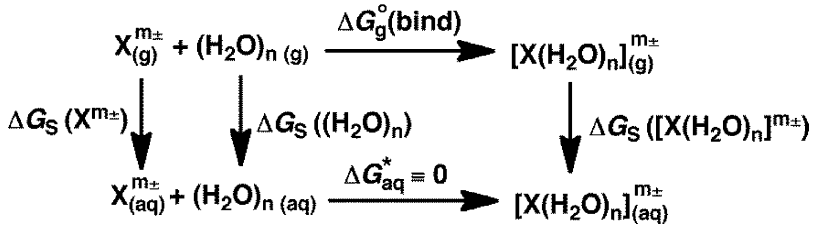

dx.doi.org/10.1021/ct300295g | J. Chem. Theory Comput. 2012, 8, 3187−3206

$= RT \ln([H_2O]/n)$,[100] where $[H_2O] = 55.34$ M. The overall expression to compute the implicit/explicit $\Delta G_S(X^{m\pm})$ value is $\Delta G_S(X^{m\pm}) = \Delta G_S^*(X^{m\pm}) + \Delta G^{o\rightarrow *}$, using eq 6.

$$\Delta G_S^*(X^{m\pm}) = \Delta G_g^\circ(\text{bind}) + \Delta G_S^*([X(H_2O)_n]^{m\pm}) + \Delta E_{\text{aq-gas}}([X(H_2O)_n]^{m\pm}) - \Delta G_S^*((H_2O)_n) - \Delta E_{\text{aq-gas}}((H_2O)_n) - RT \ln\left(\frac{[H_2O]}{n}\right) \quad (6)$$

Proton Solvation Energies. Scheme 1 requires the solvation energy of a proton in aqueous solution. This energy may be evaluated using a mixed explicit/implicit solvation model to obtain a theoretically-converged proton solvation energy (or a solvation energy for OH^- if desired). This is an arduous endeavor, however, since the integer charge found on either H^+ or OH^- will delocalize across local networks of hydrogen-bonded water molecules, so larger and larger water clusters are needed to contain the charge. H^+ does not involve any electrons so the smallest feasible model for a proton in solution would be hydronium, H_3O^+, but more physical models for a proton in solution might be Zundel ($H_5O_2^+$) or Eigen ($H_9O_4^+$) complexes.[102] Recent evidence suggests even these models are overly simplistic; infrared spectroscopic experiments by Stoyanov and Reed suggest a proton in solution is best described as a $H_{13}O_6^+$ complex, i.e., a Zundel complex embedded in four waters.[103] Alternatively, cluster-continuum cycles for pK_a calculations have been used by explicitly solvating OH^- with several water molecules.[52] In either case, calculations using so many explicit waters often run the risk of incorrectly sampling the structure of the water cluster, and it remains very difficult (if not impossible) to identify the lowest energy structures in practice.[34]

Numerous empirical values for $\Delta G_S^*(H^+)$ have appeared in the literature over the past decades.[52] There is consensus that the cluster ion experiments by Tissandier et al.[104] currently provide the most accurate value of $\Delta G_S^*(H^+) = -265.9 \pm 2$ kcal/mol, and this value has been reproduced with quantum mechanics calculations in tandem with implicit/explicit solvation models.[100,105] In their paper, however, Tissandier et al. reported a solvation energy referenced to the 1-atm standard state, $\Delta G_S^*(H^+) = -264.0$ kcal/mol, which already includes the $\Delta G^{o\rightarrow *}$ contribution described above. Camaioni and Schwerdtfeger explicitly addressed this point;[106] however, one can still find modern studies in the literature that use an incorrect proton solvation energy $\Delta G_S^*(H^+) = -264.0$ kcal/mol, presumably because incorrectly adding a second $\Delta G^{o\rightarrow *}$ term makes some calculations agree better with experiment.

One way to avoid using a disputable proton solvation energy employs a different thermodynamically-consistent cycle with isodesmic reactions based on a reference pK_a value (Scheme 4). Here, pK_as are calculated with eq 7, the aqueous-phase deprotonation energy is shown in eq 8, and ΔG_S values are obtained from eq 3.

$$pK_a = \frac{\Delta G_{aq}^*(\text{II})}{2.303 \cdot RT} + pK_a[\text{reference}] \quad (7)$$

$$\Delta G_{aq}^*(\text{II}) = \Delta G_g^\circ(\text{II}) + \Delta G_S(\text{B}) + \Delta G_S(\text{RefH}^+) - \Delta G_S(\text{BH}^+) - \Delta G_S(\text{Ref}) \quad (8)$$

Scheme 4. Isodesmic Thermodynamic Cycle to Compute the pK_a for a Conjugate Acid, BH^+

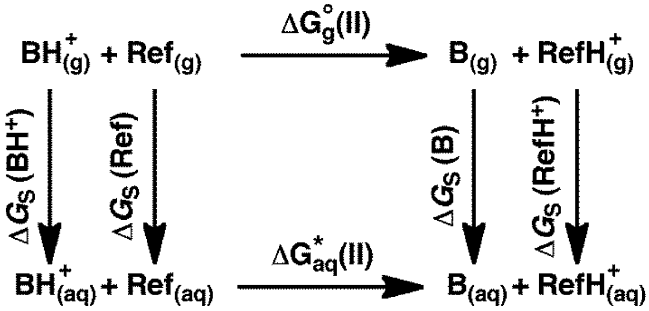

Scheme 4 does not eschew empiricism, but the isodesmic construction allows more error cancellation.[51,52] Using Scheme 4 is recommended whenever a reference pK_a for a molecule with a similar chemical moiety is available. Below we compare results for pK_a calculations of pyridinium species for which experimental data are available, using both Schemes 1 and 4. Since our ultimate goal is to report *unknown* radical pyridinyl acidities, only the cycle shown in Scheme 1 will be applicable, but comparing results from Schemes 1 and 4 will allow us to gauge expected uncertainties in our predictions for the pyridinyl pK_as.

Solvation Energies from Implicit Solvation Models. Performing implicit solvation calculations requires setting several user-defined parameters beyond selecting an appropriate basis set and level of theory for the ΔG_g° computation. Most implicit solvation calculations construct and then iteratively solve an effective Hamiltonian whereby the electrostatic problem (the Poisson equation) is solved by considering a dielectric interacting with a cavity surface that surrounds the electron density of the molecule.[14] The actual ΔG_S^* value from a solvation calculation is the energy difference between two separate calculations run by the solvation module using the same level of theory and basis set (e.g., a Restricted Hartree–Fock (RHF)/6-31G* calculation on a closed shell molecule). The module first computes a single- (structural) point self-consistent field (SCF) gas-phase reference energy, and then it computes the energy of the effective Hamiltonian using the electronic densities of the solvated orbitals. Although the solvation modules use a consistent level of theory and basis set in its calculation of ΔG_S^*, solvation energies from one specific level of theory and basis set are routinely paired with ΔG_g° values of another level of theory and basis set. Indeed, while accurate gas-phase electronic energy calculations require robust combinations of level of theory and basis set (e.g., DFT-B3LYP/aug-cc-pVDZ (aVDZ) or larger when involving a hydrocarbon), implicit solvation models are typically parametrized to give accurate results with more modest combinations of level of theory and basis set (e.g., RHF/6-31G* for the same hydrocarbon case would likely be appropriate).[92]

The cavity used in solvation calculations can be defined with different schemes, but the most robust models construct cavities with overlapping spheres centered on atoms. The individual spheres are typically based on empirically-scaled Pauling[107] or Bondi[108] van der Waals (vdW) radii or overlapping beads centered on functional groups (as constructed with United Atom Hartree–Fock (UAHF) or United Atom Kohn–Sham (UAKS) radii).[109] These cavities allow the electron density of the molecule to interact in a more physically

realistic way with the surrounding medium than those from spherical or ellipsoidal models.

The electrostatic problem can be solved on that cavity surface by finite differences (e.g., with the DelPhi solver[110]) or finite elements (e.g., with Jaguar's PBF[111,112] or the APBS program[113]), or with Green's functions (e.g., with IEFPCM[114] or SS(V)PE[115] models). COSMO models,[116,117] and its variant, CPCM,[118] first treat the solvent as a conductor (so that electrostatics are simplified) and then scale resultant energies back to values representative of real dielectrics. The electrostatic problem can also be tackled by solving the Generalized-Born equation (itself an approximation to the Poisson equation) with parametrized atom-specific data, as is done in the solvation models of Cramer and Truhlar.[15,119] ΔG_S^* energies defined by implicit solvation models typically include empirically-derived nonelectrostatic energy contributions to address the work attributed to cavitation, dispersion, and repulsion energies. The parametrization schemes for these nonelectrostatic energy terms are not always straightforward, and they are usually included to render accurate solvation energies from computationally inexpensive calculations using low levels of theory with small basis sets.[13,92]

There are ongoing discussions in the literature over which methodologies are 'best';[120,121] however, as long as these models are used correctly, most appear capable of yielding reasonable solvation energies. Since all solvation models involve empiricism (at least as part of the cavity definition if not in the overall parametrization of the model itself), all models should be rigorously tested against experimental observables before they are used for prediction of unknown properties.

COMPUTATIONAL METHODS

Unless otherwise noted, all calculations presented in this work were obtained using GAMESS-US,[122,123] a quantum chemistry code available with a free license. Electronic energies for molecules were calculated with *ab initio* HF theory[124,125] and DFT using the B3LYP exchange-correlation functional.[126,127] The default B3LYP functional in GAMESS-US uses the VWN5 correlation functional (p 1209 of ref 128). We compared differently-sized basis sets ranging from medium-sized Pople 6-31G*[129] up to the substantially larger Dunning aVDZ and aVTZ basis sets.[130] SCF calculations were considered converged once variations between the SCF densities at consecutive iterations were less than 1.0×10^{-6} electrons/bohr.[3] We also ran benchmarks at a much higher level of theory to verify the quality of our calculation scheme that largely relies on DFT-B3LYP. We report single-point electronic energies (using DFT-B3LYP/aVDZ optimized geometries) calculated using explicitly correlated (U)CCSD(T)-F12 theory[131] within the Molpro code.[132] Explicitly correlated methods using appropriate density-fitted correlation-consistent basis sets[133−135] converge much faster to the complete basis set (CBS) limit than standard calculations, leading to considerably improved accuracies within a given basis set.[131]

All geometries (including those optimized with the implicit solvation model turned on during gradient calculations) were optimized so that the largest component of the gradient was less than 1.0×10^{-5} hartree/bohr, while the rms gradient was considered converged at less than 1/3 this value. (The selected energy and gradient convergence criteria are one order of magnitude tighter than the default criteria in GAMESS-US.) Ground state geometries in gas and solvent phase were confirmed to be true minima with a vibrational frequency calculation yielding no imaginary frequencies. Zero-point energies (ZPEs) and absolute gas-phase H_{298} and G_{298} values from standard statistical thermodynamics ideal-gas-rigid-rotor-harmonic-oscillator (IGRRHO) approximations[136] were obtained using vibrational frequencies scaled with the appropriate scaling factors (to account for anharmonicity) taken from the NIST computational chemistry database.[137]

The difficulties characterizing the electronic structures of metastable radical anions have been well-documented.[83,84] Challenges arise because the energy of the electron in the HOMO of the radical is *higher* in energy than that of a free electron. As a result, the SCF calculations (from either *ab initio* HF or DFT) using sufficiently large basis sets typically converge to highly delocalized states not corresponding to resonance states observable by electron transmission spectroscopy (ETS). Several recently published procedures can be used to avoid these unwanted delocalized states, but they rely on empiricism,[138] extrapolation procedures,[139] or they assume virtual orbital energies from single-reference calculations are meaningful.[140] When dealing with radical anions that are unstable in gas phase, we find it sufficient to simply optimize their geometries while constraining the symmetry of the KS Slater determinant to the states defined by their $^2B_1$ or $^2A''$ irreducible representations, corresponding to their respective C_{2v} or C_S geometries found using the Jaguar code.[141] More details on these calculations are provided later on.

We compared three different models implemented within GAMESS-US to treat solvation effects. The SMD model[119] (as solved within the CPCM protocol of GAMESS-US) uses its own specific cavity definition and has been reported to provide reliable results using electron densities derived from a variety of levels of theory and basis set sizes. We also considered two other CPCM models using cavities defined by Bondi vdW radii[108] or S(Simplified) UAHF radii as implemented in GAMESS-US. Unlike normal UAHF radii,[109] which are defined based on chemical functional group and specifically parametrized for use at the HF/6-31G* level of theory for neutrals and cations and the HF/6-31+G* level for anions, SUAHF radii are atom-specific, meaning one sphere designates each heavy atom that is not hydrogen, regardless of the functional group in which that atom resides. Cavities were calculated using the customary scaling factor of 1.2 for all radii.[14]

ΔG_S^* values can be obtained from SMD or standard CPCM calculations and expressed in two different ways: 1) using only electrostatic (ES) energy contributions (sometimes classified as electrostatic energy plus 'delta', where the latter is the energy difference of the gas-phase Hamiltonian evaluated with solvated orbitals minus the normal gas-phase energy) or 2) the ES terms plus empirical nonelectrostatic contributions. We also note that solvation method discussions often have been prefaced by stating that ΔG_S^* should be used only within a single-point HF energy calculation with a relatively small basis set.[13,92] For calculations on radicals, this could raise issues of spin contamination within unrestricted HF (UHF) theory. Thus, we also investigated the relative importance of this by considering electron densities obtained from UDFT-B3LYP and restricted open-shell HF (ROHF) calculations as well as from larger basis sets (up to the aVDZ size).

Table 1 should be used as a key to classify the level of theory used to obtain ΔG_g° and ΔG_S^* values used to compute aqueous-phase deprotonation energies reported in upcoming figures. For example, the shorthand notation 'E1//G1' indicates deprotonation energies from DFT-B3LYP/aVTZ energy

Table 1. Quantum Chemical Calculations Used in Computations of ΔG_g^o and ΔG_S^* Given with the Shorthand Notation Used in the Text[a]

label	level of theory	basis set	solvation model	notes
Gas-Phase Electronic Energies				
E1	DFT-B3LYP	aVTZ		[b]
E2	DFT-B3LYP	aVDZ		[b]
E3	DFT-B3LYP	6-31+G**		[b]
E4	DFT-B3LYP	6-31G**		
E5	DFT-B3LYP	6-31G*		
E6	RHF	6-31G*		
E7	CCSD(T)-F12	aVDZ		[c]
Gas-Phase Geometry Optimizations and Frequency Calculations				
G1	DFT-B3LYP	aVTZ		[b]
G2	DFT-B3LYP	aVDZ		[b]
G3	DFT-B3LYP	6-31+G**		[b]
G4	DFT-B3LYP	6-31G**		
G5	DFT-B3LYP	6-31G*		
G6	RHF	6-31G*		
Single-Point Solvation Energy Calculations				
SMD1	DFT-B3LYP	aVTZ	SMD	
SMD2	DFT-B3LYP	aVDZ	SMD	[b]
SMD3	DFT-B3LYP	6-31+G**	SMD	
SMD4	DFT-B3LYP	6-31G**	SMD	
SMD5	DFT-B3LYP	6-31G*	SMD	
SMD6	RHF	6-31G*	SMD	
VDW1	RHF	aVTZ	CPCM-vdW	
VDW2	RHF	aVDZ	CPCM-vdW	
VDW3	RHF	6-31+G**	CPCM-vdW	
VDW4	RHF	6-31G**	CPCM-vdW	
VDW5	RHF	6-31G*	CPCM-vdW	
UA1	RHF	6-31G*	CPCM-SUAHF	[d,e]
UA2	DFT-B3LYP	6-31G*	CPCM-SUAHF	[b,e]
Solvent Optimized Geometry Calculations				
Gs1	DFT-B3LYP	aVDZ	SMD	[b]
Gs2	DFT-B3LYP	6-31+G**	SMD	
Gs3	DFT-B3LYP	6-31G*	SMD	
Gs4	RHF	6-31G*	SMD	
Gv1	RHF	aVDZ	CPCM-vdW	
Gv2	RHF	6-31+G**	CPCM-vdW	
Gv3	RHF	6-31G*	CPCM-vdW	
Gc1	RHF	aVDZ	CPCM-SUAHF	[d]
Gc2	RHF	6-31+G**	CPCM-SUAHF	
Gc3	RHF	6-31G**	CPCM-SUAHF	
Gc4	RHF	6-31G*	CPCM-SUAHF	
Gc5	DFT-B3LYP	aVDZ	CPCM-SUAHF	[b]

[a]Calculations on closed shell molecules used the listed levels of theory and basis sets given in the table. Calculations used for neutral and anionic radical molecules are noted in the notes column where footnotes give additional calculation details. [b]UDFT-B3LYP calculations were used for all radicals. [c]UCCSD(T)-F12 calculations were used for all radicals. [d]ROHF calculations were used for all radicals. [e]6-31+G* basis set was used for radical anions.

calculations evaluated at DFT-B3LYP/aVTZ gas-phase geometries including DFT-B3LYP/aVTZ zero-point and thermal energies in its H_{298} and G_{298} computations. Likewise, 'E7//G2' denotes deprotonation energies from single-point CCSD(T)-F12/aVDZ energy calculations evaluated at DFT-B3LYP/aVDZ gas-phase geometries including DFT-B3LYP/aVDZ zero-point and thermal energies.

ΔG_S^* values used in Schemes 1 and 4 were evaluated as single-point SMD, CPCM-vdW, or CPCM-SUAHF solvation energy calculations taken at geometries either optimized in gas phase or in solvent phase. For example, 'SMD1//G1' indicates a single-point SMD solvation energy calculation using DFT-B3LYP/aVTZ electron densities evaluated at DFT-B3LYP/aVTZ gas-phase geometries. 'VDW3//Gv2' denotes a CPCM-vdW solvation energy calculation calculated using RHF/6-31+G** electron densities calculated at the RHF/6-31+G** solvent-optimized geometry (with the CPCM-vdW solvation model turned on during gradient calculations). Note that aqueous-phase deprotonation energies using either Scheme 1 or 4 require specification of both ΔG_g^o and ΔG_S^* values, and those combinations are denoted within the figures as ΔG_g^o:ΔG_S^*. For example, data listed as 'E2//G2:UA1//Gc3' means ΔG_{aq}^* energies using 'E2//G2' ΔG_g^o values and 'UA1//Gc3' ΔG_S^* values.

After showing miniscule differences of CPCM-SUAHF solvation energies evaluated from DFT and RHF electron densities (within this data set), we later adopted CPCM-SUAHF calculations calculated with (U)DFT electron densities for closed shell (and radical) species. We will show later that electron densities calculated from UHF or ROHF calculations are not recommended when calculating solvation energies of metastable anions. We also will demonstrate later that within our closed shell molecule data set, solvent-optimized geometries are largely insensitive to the basis set used in their optimization. However, we do find that ΔG_S^* values from solvent-optimized geometries generally provide more accurate ΔG_{aq}^* energies.

In what follows, figures report the following calculation statistics with respect to the benchmark (experiment for pyridines; CCSD(T)-F12 for pyridinyls) data set: MAD − mean absolute deviation ($1/n\sum_{i=1}^{n}|x_i - x_{ref}|$); SD − standard deviation; MAX − maximum absolute deviation.

RESULTS AND DISCUSSION

Benchmarking against Closed-Shell Species. *Gas-Phase Pyridinium Deprotonations.* We calculated gas- and aqueous-phase deprotonation energies for 22 different substituted pyridine species involving one or two substituents of electron-donating methyl, ethyl, or amino groups or electron-withdrawing chloro or formyl groups. The complete data set is shown in Figure 1.

Casanovas et al.[31] used a similarly large data set in their recent study on substituted pyridines; however, more than half of their data set included carboxylic acids and hydroxide groups for which gas-phase experimental data are not available. Instead of comparing results to experiment, they used CBS-QB3 thermochemical calculations of the ΔG_g^o values in their thermochemical cycles. Thermochemical calculation procedures such as G*n*,[142−145] W*n*,[146,147] and CBS,[148−152] are well established to give accurate ΔG_g^o values, and many studies reporting calculated pK_as use them.[31,52,153−155] Accurate absolute pK_as have also been predicted using ΔG_g^o values from standard DFT methods,[27,45,156,157] and we focused on these methods since larger scale simulations will make most other thermochemical calculations prohibitively expensive. Specifically, we identified when error cancellation between ΔG_g^o and ΔG_S values leads to the highest accuracy in ΔG_{aq}^* values compared to experiment.

The Hunter and Lias reference gives definitive gas-phase deprotonation energies.[158] Their paper includes details as to how experiments are performed and states that the listed data have uncertainties of ∼8 kJ/mol or ∼2 kcal/mol (p 425 of ref

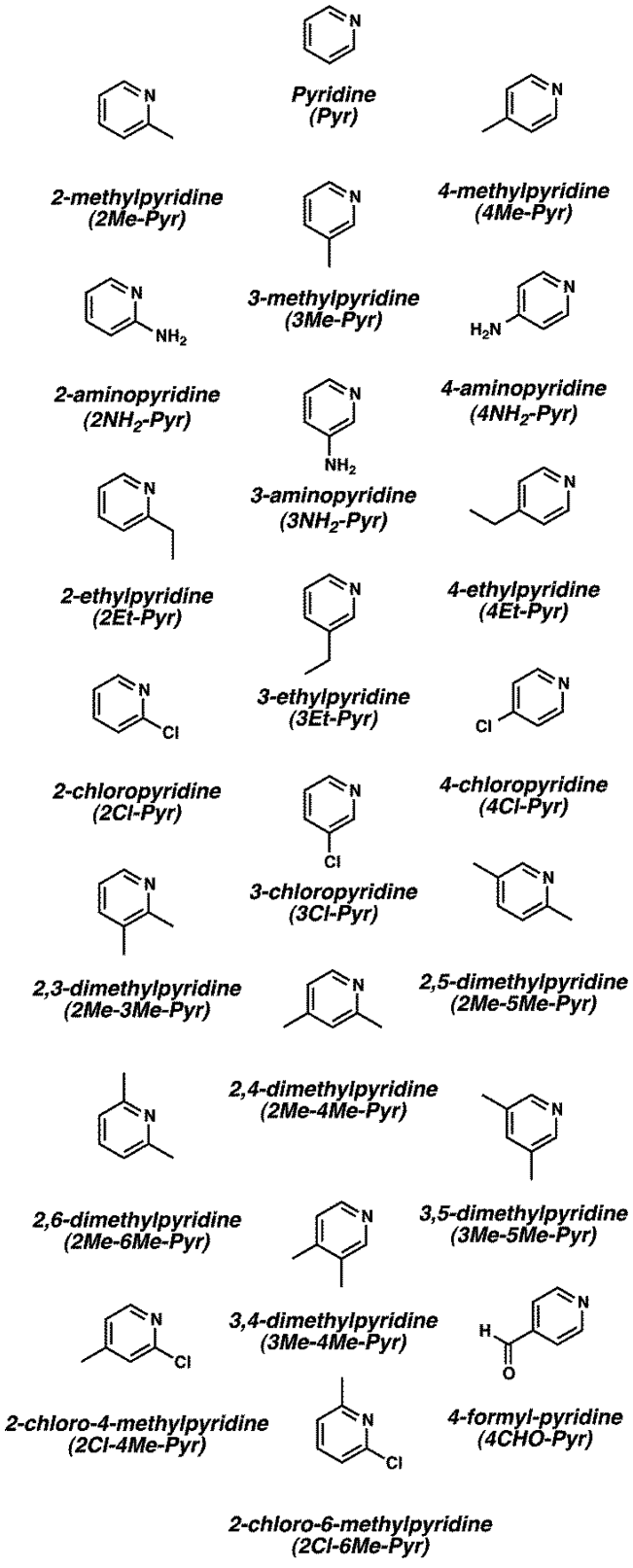

Figure 1. Substituted pyridines used in this study.

158). Using the gas-phase deprotonation analog to that shown in Scheme 1, we calculated deprotonation energies using empirical values for absolute H_{298} and G_{298} for a gaseous proton: H_{298} = 5/2 RT = 1.48 kcal/mol; G_{298} = H_{298} − $T{\cdot}S_{298}$= −6.3 kcal/mol, where S_{298} = 26.040 cal/(mol K) was taken from the Sackur-Tetrode equation.[159] Our results compared quite favorably to experimental values, as shown in Figure 2.

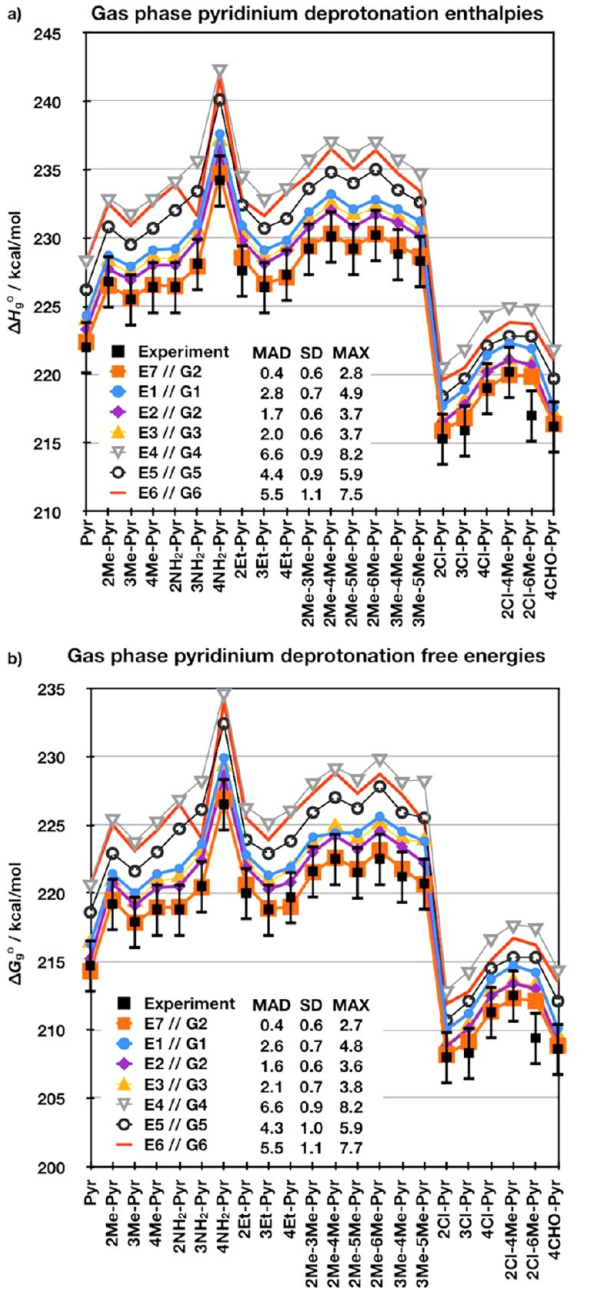

Figure 2. Gas-phase deprotonation enthalpies (a) and free energies (b) for substituted pyridinium cations. Error bars denote experimental uncertainties in gas-phase energies of 2 kcal/mol.[158] See the Computational Methods section for details and Table 1 for explanation of labels.

Figure 2 showcases two points: 1) all calculations capture the qualitative trends for experimental gas-phase deprotonation energies (e.g., the large drop in deprotonation energy once an electron-withdrawing group is present (right-hand side of plot) and 2) all DFT-B3LYP calculations (labels 'E1//G1' through 'E5//G5' in Figure 2) consistently overestimate ΔG_g^o energies. Not surprisingly, explicitly correlated CCSD(T)-F12/aVDZ ('E7//G2') provides the highest accuracy of the methods tested (MAD = 0.4 kcal/mol; SD = 0.6 kcal/mol; MAX = 2.7 kcal/

dx.doi.org/10.1021/ct300295g | J. Chem. Theory Comput. 2012, 8, 3187−3206

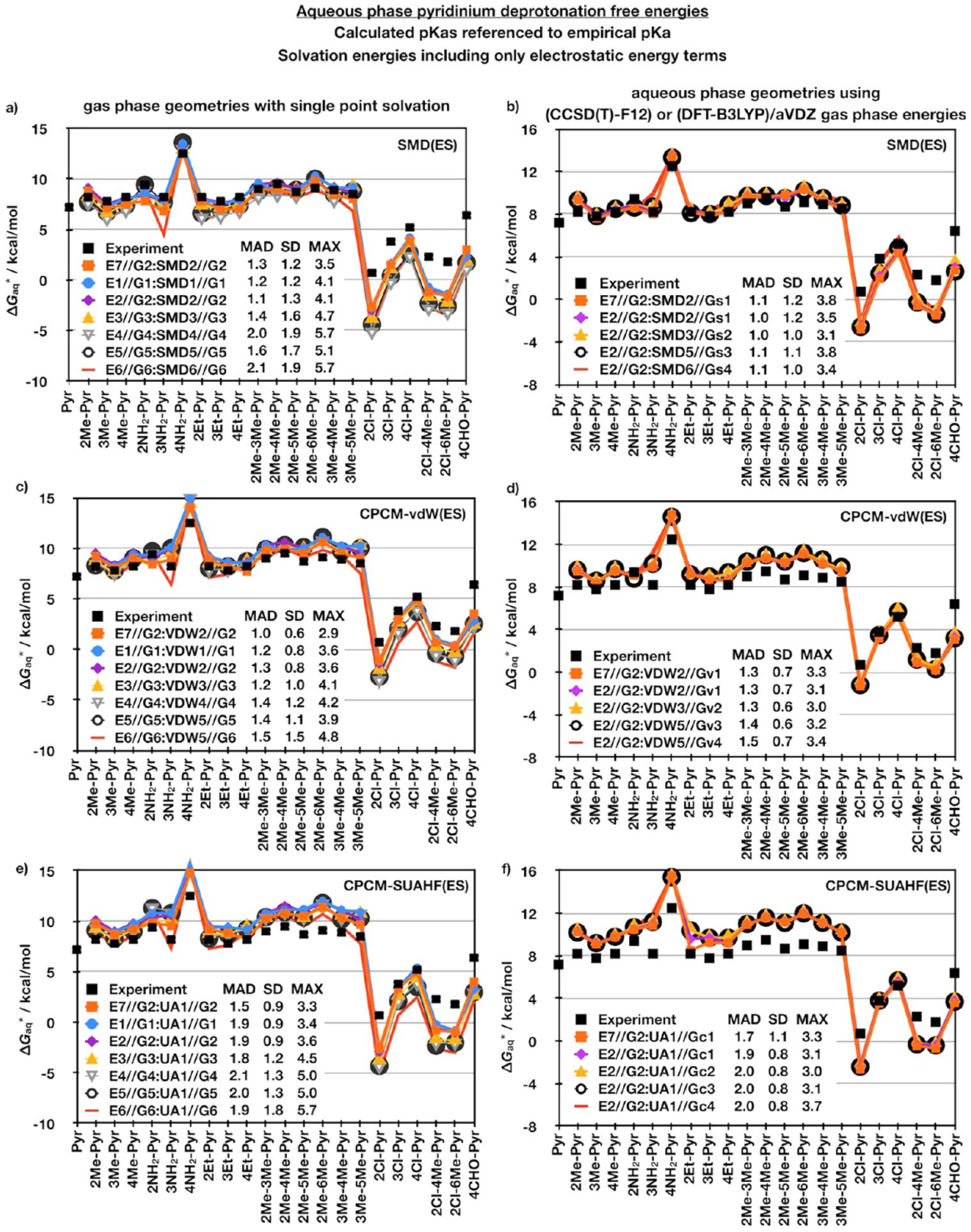

Figure 3. Aqueous-phase deprotonation energies (ΔG^*_{aq}) for substituted pyridinium cations as calculated with the thermodynamic cycle in Scheme 4. Charts on the left use gas-phase optimized structures for ΔG^*_S values, while charts on the right use solvent-phase optimized structures for ΔG^*_S values. See the Computational Methods section for more details and Table 1 for explanation of labels.

mol). Of the DFT calculations, DFT-B3LYP/aVDZ ('E2//G2') is the next closest to matching experiment (MAD = 1.6 kcal/mol; SD = 0.6 kcal/mol; MAX = 3.6 kcal/mol). Across the entire data set, error statistics are nearly the same for ΔH^o_g and ΔG^o_g energies, indicating that the IGRRHO treatment of the $T\Delta S_{298}$ term in the ΔG^o_g energies is justified for these deprotonations. Note also that the two most accurate methods, CCSD(T)-F12/aVDZ and DFT-B3LYP/aVDZ ('E7//G2' and 'E2//G2'), both find deprotonation energies for **2Cl-6Me-Pyr** to be ~2.5 kcal/mol higher than experiment, suggesting this particular measurement may require re-evaluation. HF/6-31G* ('E6//G6'), the specified level of theory and basis set for neutral and cation solvation calculations using UAHF cavities, produces gas-phase deprotonation energies consistently ~5.5 kcal/mol larger than experiment, except for **3NH$_2$-Pyr**, which is calculated within ~3 kcal/mol of experiment. DFT-B3LYP/6-

dx.doi.org/10.1021/ct300295g | J. Chem. Theory Comput. 2012, 8, 3187−3206

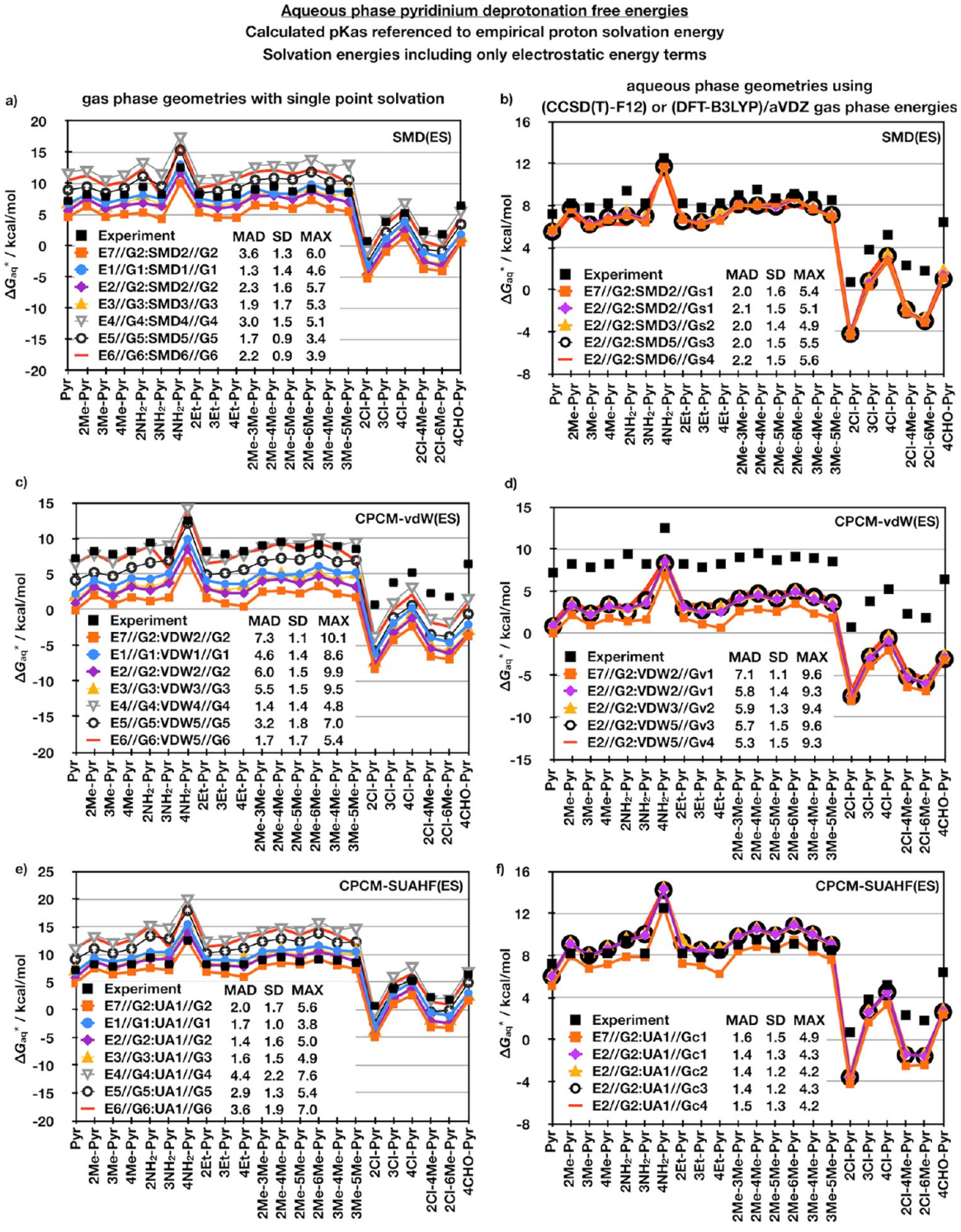

Figure 4. Aqueous-phase deprotonation energies (ΔG^*_{aq}) for substituted pyridinium cations as calculated with the thermodynamic cycle in Scheme 1. Charts on the left use gas-phase optimized structures for ΔG^*_S values, while charts on the right use solvent-phase optimized structures for ΔG^*_S values. See the Computational Methods section for more details and Table 1 for explanation of labels.

31G* calculations ('E5//G5') provide a more consistent description of these deprotonation energies with **3NH$_2$-Pyr** no longer an outlier, but energies are consistently ~4.5 kcal/mol too high. Interestingly, the additional *p* polarization function on H atoms in B3LYP/6-31G** calculations ('E4//G4') cause a noticeable degradation in accuracy, leading to results even worse than those obtained at the HF/6-31G* ('E6//G6') level. Note that the 6-31G** basis set is often a default basis set in quantum chemistry calculations. Although none of these calculations involved anionic species, one sees dramatic improvement once diffuse ('+') functions are added to the basis set. Evidently, since these deprotonations occur at the relatively electronegative nitrogen, diffuse functions are needed for accuracy. The aVDZ basis set is substantially larger but shows only modest improvement over the 6-31+G** basis set. The even-larger basis set, aVTZ, now shows signs of basis set

dx.doi.org/10.1021/ct300295g | J. Chem. Theory Comput. 2012, 8, 3187−3206

saturation and gives results with slightly lower accuracy than aVDZ and 6-31+G** basis sets. Thus, we consider the aVDZ basis set is converged with respect to DFT-B3LYP ΔG_g^o values.

We briefly summarize related data given in the Supporting Information. We report DFT calculated deprotonation reaction energetics from pyridinium cation (Figure S1) and pyridine itself (Figure S2). DFT-B3LYP/aVDZ//DFT-B3LYP/6-31G** and DFT-B3LYP/aVDZ//DFT-B3LYP/6-31+G** calculations almost exactly reproduce fully optimized DFT-B3LYP/aVDZ energies. Scaled vibrational frequencies in these calculations provide very small improvement in deprotonation energies (errors due to $T\Delta S_{298}$ are decreased on average by 0.1 kcal/mol, Figure S3). As expected, closed-shell gas-phase pyridinium and pyridine deprotonations are well behaved. Although DFT-B3LYP/6-31G** ΔG_g^o values are quite poor, their geometries and frequencies are sufficient for ΔG_g^o calculations when using larger basis sets for the electronic energies.

Aqueous-Phase Pyridinium Deprotonations. Most experimental pK_as were obtained from the CRC Handbook or a journal reference.[160] In some cases experimental pK_as were obtained from the chemistry reference Web site, ChemicalBook.[161] Unfortunately, pK_a measurements are not always taken at the same temperature, and though potentiometric titration measurements have uncertainties ±0.03−0.05 pK_a units,[162] reference table pK_as often have higher uncertainties since they were obtained as averages of several reported values. Comparing different literature values, we note experimental pK_as can vary up to ∼0.3 pK_a units, and this corresponds to ∼0.4 kcal/mol on an energy scale. Based on these data, we found that DFT-B3LYP calculations with larger basis sets were slightly more accurate when using only ES solvation energy contributions, and so we report those values in the main text, while total solvation energy data are given in the Supporting Information in Figures S4 and S5.

First we consider the limit of maximum error cancellation using the pK_a reference cycle of Scheme 4. Here, all values are referenced relative to the experimental pK_a of pyridine, 5.3, corresponding to an experimental $\Delta G_{aq}^* = 7.2$ kcal/mol. The left-hand side of Figure 3 shows ΔG_{aq}^* ($2.303 \cdot RT \cdot pK_a$; $T = 298$ K) values using different gas-phase geometries with single-point solvation energies calculated as stated in the Computational Methods section and Table 1. The right-hand side of Figure 3 shows ΔG_{aq}^* values using DFT-B3LYP/aVDZ ('E2//G2') or CCSD(T)-F12/aVDZ ('E7//G2') ΔG_g^o values (since these were most accurate in Figure 2) and ΔG_S^* values calculated using solvent-optimized geometries to test the sensitivity of the latter to the calculation method. Figures 3a and 3b show calculations using the SMD solvation model, Figures 3c and 3d show calculations using the CPCM-vdW solvation model, and Figures 3e and 3f show calculations using the CPCM-UAHF solvation model. As expected, all three different solvation models perform similarly well when using the isodesmic calculation Scheme 4.

Figures 3a, 3c, and 3e demonstrate that ΔG_{aq}^* MAD values improve with increasing basis size; this trend is largely because the ΔG_g^o values within the overall ΔG_{aq}^* calculations dramatically improve with larger basis set size (Figure 2). The most accurate calculations compared to experiment again are those involving CCSD(T)-F12 calculations ('E7//G2') for ΔG_g^o; however, ΔG_{aq}^* MADs for those calculations are *larger* than the corresponding ΔG_g^o MADs shown in Figure 2. In contrast, combining DFT-B3LYP/aVDZ ΔG_g^o values and SMD or CPCM-vdW ΔG_S^* values lead to *smaller* ΔG_{aq}^* MADs, showing this combination benefits from error cancellation. Results using DFT-B3LYP/aVDZ and DFT-B3LYP/aVTZ ΔG_g^o values are essentially identical and both are slightly more accurate than DFT-B3LYP/6-31+G** calculations, so we favor using the aVDZ basis set when calculating ΔG_g^o. While most of these schemes shown in Figure 3a, 3c, and 3e predict reliable pK_as of methyl, ethyl, and amino (electron donating) substituents, noticeably larger errors occur when the substituents involve electron-withdrawing chlorine or formyl groups. These errors will be reduced when explicit solvation by a water molecule is included.

Figures 3b, 3d, and 3f show results comparing ΔG_S^* values from solvation-optimized structures (using similar ΔG_g^o values deemed accurate from Figure 2). ΔG_S^* values from different solvent-optimized geometries were nearly identical, regardless if the geometry optimization occurred at, e.g., the HF/6-31G* or DFT-B3LYP/aVDZ level. However, ΔG_S^* values from solvent-optimized geometries are moderately better than ΔG_S^* values from gas-phase optimizations when using DFT-B3LYP/aVDZ ΔG_g^o values. When using CCSD(T)-F12/aVDZ ΔG_g^o values with ΔG_S^* values from solvent-optimized geometries, the results are sometimes worse and sometimes better. In terms of overall pK_a accuracies, the SMD ΔG_S^* values (from solvent-optimized geometries) with CCSD(T)-F12/aVDZ or DFT-B3LYP/aVDZ ΔG_g^o values yield ΔG_{aq}^* energies on average within 1.1 kcal/mol of experiment (∼0.8 pK_a units). When calculating substituent effects on molecules not involving formyl or chlorine electron-withdrawing groups, MADs are 0.4 kcal/mol (less than 0.3 p$K_a$units). CPCM-vdW ΔG_S^* values lead to the lowest ΔG_{aq}^* SD and MAX errors since CPCM-vdW ΔG_S^* values reduce the maximum errors in Cl- and formyl-substitutions. SMD ΔG_S^* values produce the lowest ΔG_{aq}^* MAD values, showing it robustly captures aqueous-phase substituent effects of C- and N-group substituents. CPCM-SUAHF ΔG_S^* values are the least accurate of the three models when using calculation Scheme 4.

Optimization of a pK_a Calculation Scheme without an Empirical Reference pK_a. We now consider direct pK_a computation using Scheme 1, which calls for an empirical proton solvation energy (Figure 4). Since the construction of Scheme 1 is not isodesmic, ΔG_{aq}^* calculations are expected to be less accurate than the data shown in Figure 3. Although smaller basis set calculations occasionally give respectable results (*e.g.*, DFT-B3LYP/6-31G* in Figure 4a and DFT-B3LYP/6-31G** in Figure 4c), we avoided pursuing these calculations since we wanted to find the solvation calculations best suited to cancel out the systematic positive errors found in gas-phase DFT-B3LYP/aVDZ calculations. The solvent-optimized CPCM-SUAHF calculations shown in Figure 4f were the best for this purpose, providing MADs of 1.4 kcal/mol and MAX errors of 4.3 kcal/mol. Note that under this scheme, calculations using high quality CCSD(T)-F12/aVDZ gas-phase energies are less accurate than those from the more economical DFT-B3LYP/aVDZ calculations (again, error cancellation is obviously playing a role).

Spin contamination often plagues UHF calculations[124,125] on radicals,[163] and electron densities from spin-contaminated calculations should not be trusted. Therefore, we considered using ΔG_S^* values from DFT electron densities since those are less susceptible to spin contamination. Based on Figure 5a, CPCM-SUAHF ΔG_S^* values using either DFT or RHF electron densities are nearly identical − the MAD, SD, and MAX errors between the two differ by only 0.1 kcal/mol. This is an insignificant difference, and since all gas-phase calculations

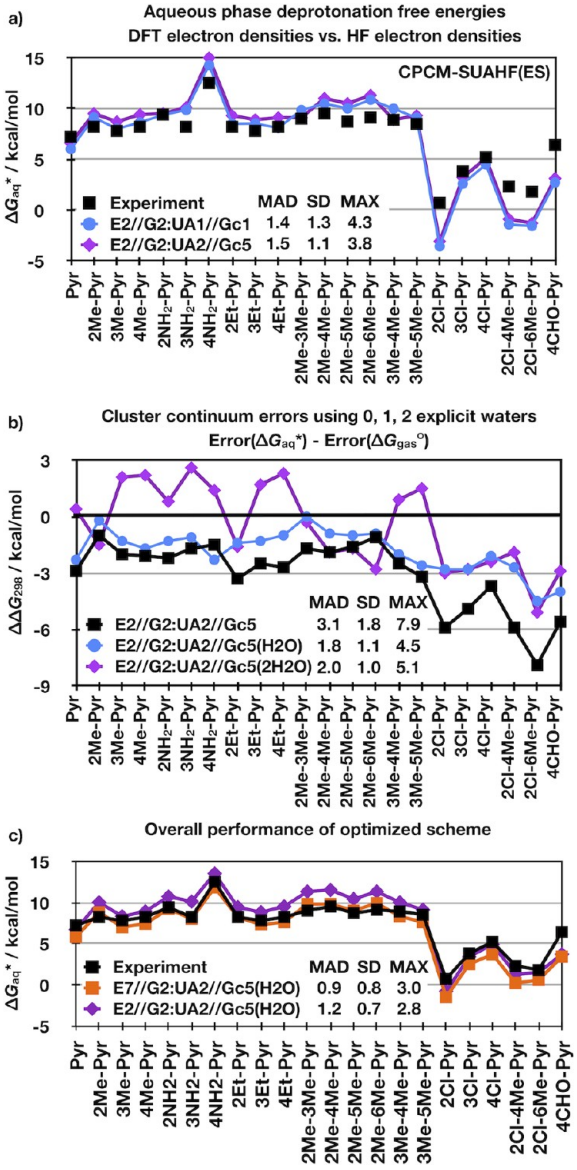

Figure 5. (a) A comparison of aqueous-phase deprotonation free energies (ΔG^*_{aq}) for substituted pyridinium cations using ΔG^*_S values from RHF ('UA1/Gc1') and DFT-B3LYP ('UA2/Gc5') electron densities. (b) Errors in the cluster-continuum solvation model reported as aqueous-phase deprotonation energy errors minus gas-phase deprotonation energy errors for substituted pyridinium cations plotted for different numbers of explicit water molecules. (c) Performance of the final optimized solvation approach used in this study. See the Computational Methods section for more details and Table 1 for explanation of labels.

already use DFT-B3LYP geometries, all subsequently reported solvation energies use electron densities from UDFT-B3LYP/6-31G* calculations (for pyridinyls) and UDFT-B3LYP/6-31+G* (for pyridine radical anions).

Our last benchmarking considered the role of mixed implicit/explicit solvation. Several different approaches exist to determine a suitable number of water molecules for accurate ΔG^*_S. One approach is to use the quasichemical theory of Pratt to obtain the entire first solvation shell of a solute molecule.[164] Alternatively, one could use a fixed number of water molecules after determining their lowest energy conformation from molecular dynamics simulations, e.g., using five explicit water molecules, as was done by da Silva et al.[165] A third approach is to use the cluster-continuum solvation approach (Scheme 3) and add water molecules until solvation energies are converged.[101]

In most of our cases, each pyridine species can be classified as a hydrophobic hydrocarbon with only one significant hydrogen-bonding site, the pyridine sp^2 nitrogen. Even though the position of at least the first water molecule is straightforward to determine uniquely, we began adding water molecules near the sp^2 nitrogen as well as at other heteroatom sites, optimizing their geometries in the gas phase as well as under the influence of solvation. Indeed, water binds most strongly at the sp^2 N site in all pyridine and pyridinium molecules (including those with amino-substituted groups). The second water molecule preferentially binds to the first N-bonded water molecule rather than any other site around the ring.

Since we were primarily interested in ΔG^*_{aq} and not ΔG^*_S values, we benchmarked our calculations against deprotonation energy errors (with respect to experiment) for aqueous-phase (Figure 4f) minus gas-phase (Figure 2b) calculations. We report the errors in solvation models involving 0, 1, and 2 explicit H_2O molecules (Figure 5b), where the aqueous-phase deprotonation energies calculated using Scheme 1 involved the same number of water molecules in both the protonated and deprotonated species. Adding one explicit water (so that it forms an O−H...N hydrogen bond to pyridine or a O...H−N hydrogen bond to pyridinium) improves ΔG^*_{aq} accuracies overall. The largest corrections from the added water (resulting in corrections ranging from 2−3 kcal/mol) occur when the pyridinium has electron-withdrawing Cl or CHO groups. ΔG^*_{aq} values particularly improve when Cl resides at *ortho*-positions, i.e., when Cl atoms are adjacent to the H-bonding site. Although water prefers to form an H-bond only to the N-atom and not to the Cl, adding the explicit water to the calculation improves the accuracy by 3.1, 3.2, and 3.5 kcal/mol for the ΔG^*_{aq} values involving **2Cl-Pyr**, **2Cl-4Me-Pyr**, and **2Cl-6Me-Pyr**, respectively. For electron-donating groups (even with *ortho*-substituted CH_3 or NH_2 groups) the explicit water does not significantly change the overall solvation energy. The preferential binding site of one water molecule to pyridine or pyridinium is unambiguous with the CPCM-(S)UAHF model. The first explicit water always binds most strongly to the N-terminus of the pyridine (or the N−H bond of pyridinium). Because (S)UAHF cavities do not explicitly account for hydrogen atoms, the orientation of the first water does not affect the solvation energy. However, when a second explicit water molecule is added to the calculation, forming a water dimer bound to the sp^2 N, errors fluctuate between values close to those with one H_2O and values near +3 kcal/mol. We attribute this to inadvertently using higher energy orientations of the water dimer in some calculations. Presumably, rigorously using any of the three implicit/explicit approaches mentioned earlier should lead to accurate results; however, our results in Figure 5b showed a sizable improvement by adding only one explicit water molecule (Figure 5b); thus, our final reported energies only include one explicit water.

Having completed this solvation scheme optimization to study substituted pyridinium deprotonations, our best-performing methodology is shown in Figure 5c. The error statistics for the entirely DFT-based scheme ('E2//G2:UA2//Gc5(H2O)': MAD = 1.2 kcal/mol, SD = 0.7 kcal/mol, MAX = 2.8 kcal/mol) compare very well to similar calculations using CCSD(T)-F12/aVDZ gas-phase energies ('E7//G2:UA2//Gc5(H2O)': MAD

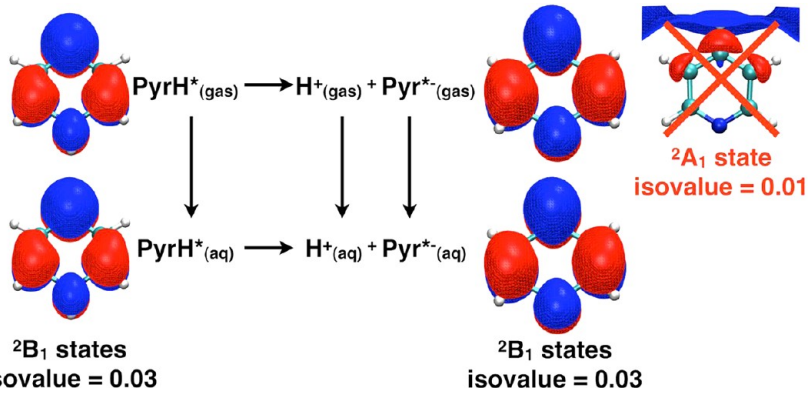

Figure 6. Radical states for species involved in pK_a calculations. The ground state for protonated pyridinyl (PyrH*) is the $^2B_1$ electronic state, while the calculated ground state of gas-phase pyridine radical anion (Pyr^{*-}) will be the $^2A_1$ state unless constraints are imposed. 'Isovalue' refers to the HOMO amplitude isosurface value (red positive, blue negative).

= 0.9 kcal/mol, SD = 0.8 kcal/mol, MAX = 3.0 kcal/mol), giving us confidence in predicting pK_as for pyridinyl radical species next.

Pyridinyl Radical pK_as. Radical deprotonations are defined with a similar scheme as closed shell deprotonations. A significant difference now is that neutral radical deprotonations result in a negatively charged anion radical (eq 9). The fact alone that it is an anion is not grounds for concern since DFT-B3LYP/aVDZ does an equally good job calculating ΔG_g^o for closed-shell cations as well as for neutral species (see Figure S2 in the Supporting Information). Furthermore, since the deprotonations shown in eq 9 have a radical on both sides of the equation, one would expect favorable error cancellation when the electronic states of the species on both sides of the equation are similar.

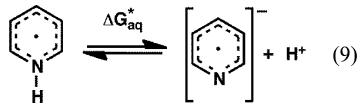

(9)

Gas-Phase Adiabatic Electron Affinities. The electron affinity for a neutral species, X, is defined as the energy cost to remove the extra electron from its anionic form (eq 10).

$$X^- \rightarrow X + e^- \quad (10)$$

Adiabatic electronic affinities can be calculated as the H_0 (electronic energy plus ZPE) of the optimized molecule without the added electron (X) minus the H_0 of the optimized molecule with the extra electron (X^-). Pyridinium cations have positive electron affinities (due to their positive charge), and the ground state of the neutral pyridinyl radical is a $^2B_1$ state (i.e., with the unpaired electron in a π-antibonding orbital). In contrast, neutral pyridine has a *negative* electron affinity because the energy of the gaseous pyridine anion is *higher* than that for neutral pyridine plus a free electron. Under these circumstances, the electronic structure for pyridine anion is nontrivial to characterize. One would expect to need a large basis set with diffuse functions to describe the more expansive electronic density of the anion, but such a basis set further complicates matters since its diffuseness also allows the calculation to potentially converge to lower-energy, highly delocalized states (i.e., with the unpaired electron largely unbound). Without artificial constraints on the optimizing orbitals, *ab initio* HF or KSDFT calculations on the pyridine radical anion will result in the lower energy delocalized $^2A_1$-like state, which is simply trying to autoionize.

The $^2A_1$-like state may be physically significant or it may just be an artifact of using diffuse basis sets. Regardless, its presence can create inconsistencies in both ΔG_g^o and ΔG_S^* values needed for pK_a calculations. Recall that ΔG_S^* values from implicit solvation models are defined as the energy from the semiempirical solvation model Hamiltonian (using solvated orbitals) minus the energy from the quantum mechanical gas-phase Hamiltonian (using gas-phase orbitals). Orbitals in the former SCF calculation usually converge to a bound valence state,[139] but orbitals in the latter SCF calculation sometimes may not. For pyridinyl radicals, this is inconsequential because the ground states of both the gas-phase and aqueous-phase species are the same. For pyridine anions, however, if one of the gas-phase energies in ΔG_g^o or the gas-phase component of ΔG_S^* optimize to different states, then errors will result due to the thermochemical cycle not being closed (see Figure 6). Note that in the C_{2v} point group, the $^2A_1$ state is delocalized/continuum-like, while the $^2B_1$ state is the bound valence state (corresponding to adding an electron to the π antibonding level). In the C_s point group, the respective labels are $^2A'$ and $^2A''$. Since the $^2A_1$-like state only appears in gas-phase pyridine radical anion calculations (the aqueous-phase ground state is always $^2B_1$-like), we focused our attention on finding gas-phase $^2B_1$-like states for those anions so as to have a properly closed thermodynamic cycle.

For some pyridine anions, the $^2B_1$-like state can be challenging to characterize. Obtaining it without extrapolation schemes requires explicitly defining the symmetry of the orbitals used in the calculation as can be done in quantum chemistry codes such as Molcas,[166] Molpro,[132] and Jaguar.[141] Once the geometry of the $^2B_1$-like state has been optimized, confirming the nature of its optimized geometry required calculating vibrational frequencies with analytic Hessian calculations, as can be done with Jaguar for DFT-B3LYP. (Analytic Hessians are required since numerical Hessians that require perturbing the $^2B_1$-like geometry will result in broken symmetry $^2A_1$-like states.) Not surprisingly, in some of our cases, the $^2B_1$-like states optimized to a transition state with one imaginary frequency (consisting of either a methyl group rotation or an amino group inversion) breaking the pyridinyl/pyridine anion plane of symmetry. Although these states do not correspond to energetic minima on the $^2B_1$-like potential energy surface, we report them anyway since the nature of their imaginary frequencies suggests these transition states are on the order of 1−2 kcal/mol from the true minimum energy point.

We now proceed to discuss results from gas-phase calculations on the $^2A_1$-like and $^2B_1$-like pyridinyl/pyridine anion states.

First, we give as much context to the quality of electron affinity calculations as possible. Nenner and Schulz determined the electron affinity of pyridine to be −0.62 ± 0.05 eV using ETS spectroscopy;[82] this is the sole piece of experimental data available with which we can benchmark our pyridine anion calculations. Based on this metric alone, the calculations we employ perform quite well—(U)CCSD(T)-F12/aVDZ and (U)DFT-B3LYP/aVDZ calculations obtained values of −0.71 eV and −0.64 eV, respectively. Comparing to even more computationally demanding basis sets shows (U)CCSD(T)-F12/aVTZ and (U)CCSD(T)-F12/aVQZ give electron affinities of −0.66 eV and −0.64 eV, respectively. Although (U)DFT-B3LYP fortuitously outperforms (U)CCSD(T)-F12 in this test case, we choose in subsequent figures to show the MAD/SD/MAX statistics relative to (U)CCSD(T)-F12/aVDZ calculations, the calculations that yielded the lowest average error in Figure 5c.

Anion calculations sometimes require particularly diffuse basis sets, and Jensen reported that metastable anions require very diffuse basis sets (with exponents as small as $\sim 1 \times 10^{-4}$) to reach convergence for electron affinities.[167] The relatively large aVTZ basis set, in contrast, has diffuse functions with exponents only as small as 2×10^{-2}. As Jensen's test set involved mainly atomic and diatomic anions, we investigated if these highly diffuse basis functions are needed in our larger molecular anions. We further augmented the aVTZ basis set within Molpro with one additional even-tempered diffuse *s* function on each atom, with exponents between 5×10^{-4} and 8×10^{-4}. (Making the diffuse *s* functions more diffuse or using multiple primitive diffuse *s* functions created convergence problems.) The new basis set was used to calculate the energies of the $^2A_1$-like and $^2B_1$-like states of the unsubstituted pyridine radical anion. Compared to the standard aVTZ basis set, the (U)DFT-B3LYP energy of the $^2B_1$-like state did not change at all, and the (U)DFT-B3LYP energy of the $^2A_1$-like state changed by only 0.02 eV, showing the more diffuse basis sets are not needed here, even when describing the highly delocalized $^2A_1$-like state.

Gas-Phase Pyridinyl Deprotonation Energies. Figure 7 summarizes gas-phase pyridine electron affinity and pyridinyl deprotonation energy predictions. Note that the **4Cl-Pyr** pyridine radical anion was calculated to autoionize with every basis set tested, so it was removed from the data set; it is known experimentally to be unstable as well.[168] Also, convergence issues due to basis set linear dependencies prevented a full study using the aVTZ basis set. Of the aVTZ calculations that converged, however, both aVDZ and aVTZ DFT-B3LYP geometries were nearly identical, and both gave similar deprotonation energies (within a MAD of 1.0 kcal/mol; see Supporting Information, Figure S6).

Figure 7a shows that $^2A_1$-like states manifest themselves only in cases *without* electron withdrawing substituents. Additionally, electron-donating substituents further stabilize the $^2A_1$-like anions relative to the unsubstituted pyridine anion. In the unsubstituted case and cases with electron-donating substituents, the CCSD(T)-F12 calculations find the $^2B_1$-like states are higher in energy than the $^2A_1$-like states by 0.2 to 0.5 eV, where the largest differences occur with ethyl- and dimethyl-substituents. DFT-B3LYP calculations find a similar trend, though energy differences are usually smaller, and in a few cases (**4Me-Pyr***, **2Me-6Me-Pyr***, and **3Me-5Me-Pyr***) the two

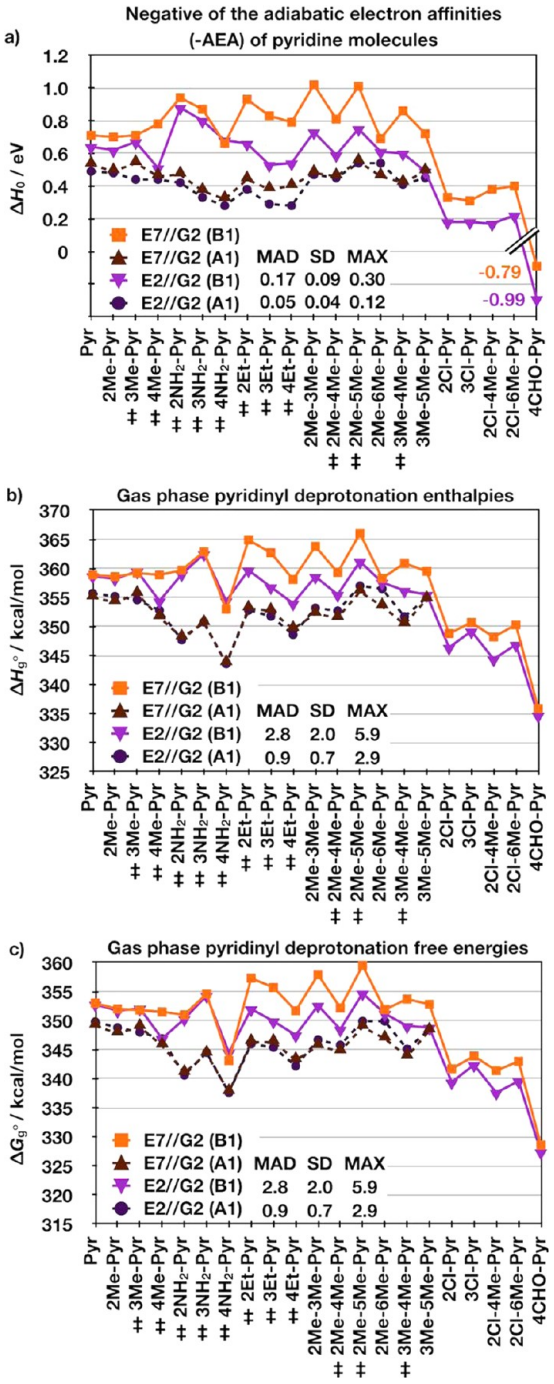

Figure 7. (Negative of the) gas-phase adiabatic electron affinities (-AEA) for substituted pyridines (a) and deprotonation enthalpies (b) and free energies (c) for substituted pyridinyl radicals. A1 and B1 denote energies involving $^2A_1$-like and $^2B_1$-like pyridine anions. DFT-B3LYP 'E2//G2' MAD, SD, and MAX values are relative to corresponding CCSD(T)-F12 'E7//G2' calculations. See the Computational Methods section for more details and Table 1 for explanation of labels. The '‡' symbol denotes molecules whose $^2B_1$-like state geometry optimizations resulted in a transition state. See text for details.

states are nearly degenerate in energy. Overall, the DFT-B3LYP $^2A_1$-like states differ from the CCSD(T)-F12 $^2A_1$-like states by only 0.05 eV on average, showing surprisingly consistent agreement in capturing the energy of the delocalized states. The DFT-B3LYP $^2B_1$-like states, however, differ somewhat more

dx.doi.org/10.1021/ct300295g | J. Chem. Theory Comput. 2012, 8, 3187−3206

from the CCSD(T)-F12 $^2B_1$-like states, on average by 0.17 eV. In terms of electron affinities, the combination of electron-donating groups with additional dispersion interactions cause DFT-B3LYP electron affinities to be as much as 0.3 eV less negative than those from CCSD(T)-F12 calculations. For the electron-withdrawing substituents, a single chlorine substituent still causes pyridine to have a negative electron affinity (∼−0.35 eV and ∼−0.20 eV in CCSD(T)-F12 and DFT-B3LYP calculations, respectively). Notably, the electron affinity of **4CHO-Pyr** is quite positive compared to the other cases, showing it is energetically favorable to add an electron to this substituted pyridine.

The trends in energies highlighted in Figure 7a arise again in Figure 7b and Figure 7c, thus showing how the differences in ΔG_g^o are mainly governed by the stability of the pyridine anion. Similar to that shown in Figure 2, ΔG_g^o values in Figure 7b and Figure 7c vary within a similar range of ∼30 kcal/mol. However, the deprotonation energies for pyridinyl species are ∼135 kcal/mol *higher* than those for the corresponding pyridinium species: deprotonation enthalpies range from ∼335−365 kcal/mol and deprotonation free energies range from ∼330−360 kcal/mol. Pyridinyl deprotonations are very high because they generate highly unstable pyridine anions. This enormous increase in the deprotonation energy in turn causes a large decrease in the acidities of these species, as we now discuss.

Aqueous-Phase Pyridinyl Deprotonation Energies. Having distinguished between the $^2A_1$-like and $^2B_1$-like states for the gas-phase pyridinyl radicals, we now report ΔG_{aq}^* results. Figure 6 illustrates how unintentionally converging to the $^2A_1$-like state rather than the $^2B_1$-like state creates an inconsistency in the thermodynamic cycle. Most likely, this inconsistency will occur when the radical anion gas-phase energy within ΔG_g^o (using a large and flexible basis set, e.g., aVDZ) converges to the $^2A_1$-like state, while the gas-phase reference energy of the ΔG_S^* calculation (which frequently uses a smaller, less flexible basis set, e.g., 6-31+G* or smaller by construction) converges to the $^2B_1$-like state. Note that we always find that the final solvated state in the ΔG_S^* calculation is the $^2B_1$-like state. Thus, without paying careful attention to the electronic states obtained, the thermochemical cycles used in acidity calculations may sometimes omit an energy term linking the gas-phase energies of the $^2A_1$-like and $^2B_1$-like states, and we previously showed this difference can be as large as 0.5 eV = 11.5 kcal/mol = 8.4 pK_a units. Using a smaller basis set for ΔG_S^*calculations on similar anions is perhaps then good practice to consistently obtain the $^2B_1$-like state in the gas-phase reference (as well as in the final solvated state). This leaves the largest remaining error associated with identifying the gas-phase energy of the $^2B_1$-like state within the ΔG_g^o calculation. This suggestion is confirmed by the data shown in Figure 8, which displays a summary of solvation calculations using both DFT-B3LYP/aVDZ ('E2//G2') and CCSD(T)-F12/aVDZ ('E7//G2') gas-phase energies and a selection of differently calculated ΔG_S^* values.

Note that statistics presented in all of Figure 8 are relative to the CCSD(T)-F12 calculations shown in Figure 8c, using the optimized solvation scheme ('E7//G2:UA2//Gc5(H2O)') shown in Figure 5c. Figure 8a shows that ΔG_{aq}^* can vary substantially if gas-phase optimized structures (not including an explicit water molecule) are used for ΔG_S^* calculations. Here, CCSD(T)-F12/aVDZ calculations with CPCM solvation ('E7//G2:UA2//G2') deviate from the benchmark CCSD-(T)-F12 calculations in Figure 8c on average by 2.3 kcal/mol,

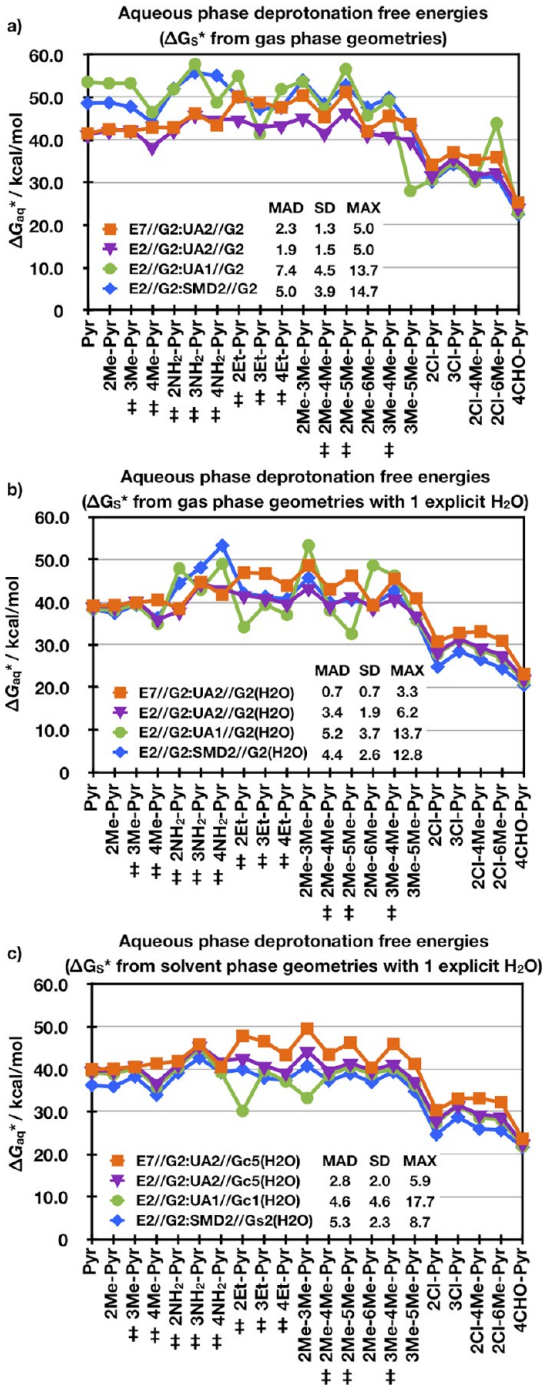

Figure 8. Pyridinyl ΔG_{aq}^* values using ΔG_S^* values based on (a) gas-phase optimized geometries, (b) gas-phase optimized geometries using one explicit water molecule, and (c) solvent-phase optimized geometries using one explicit water molecule. All deprotonations assume all pyridine anions are in a $^2B_1$-like state. All MAD, SD, and MAX values are relative to the corresponding CCSD(T)-F12 calculations using solvation energies from solvent-optimized structures with one explicit water molecule ('E7//G2:UA2//Gc5(H2O)'). See the Computational Methods section for more details and Table 1 for explanation of labels. The '‡' symbol denotes molecules whose $^2B_1$-like state geometry optimizations resulted in a transition state. See text for details.

and the maximum deviation is 5.0 kcal/mol. DFT-B3LYP/aVDZ calculations with CPCM solvation differ ('E2//G2:UA2//G2') on average by 1.9 kcal/mol, which is slightly

dx.doi.org/10.1021/ct300295g | J. Chem. Theory Comput. 2012, 8, 3187−3206

Table 2. Gas-Phase Deprotonation Enthalpies (ΔH^{o}_{g}) and Free Energies (ΔG^{o}_{g}), Aqueous-Phase Free Energies (ΔG^{*}_{aq}) of Substituted Pyridinium Cations at T = 298 K (All in kcal/mol), and Corresponding Aqueous-Phase pK_as[a]

	ΔH^{o}_{g}			ΔG^{o}_{g}			ΔG^{*}_{aq}			pK_a		
pyridinium name	exp[b]	CCSD(T)-F12	DFT-B3LYP	exp[b]	CCSD(T)-F12	DFT-B3LYP	exp[c]	CCSD(T)-F12	DFT-B3LYP	exp	CCSD(T)-F12	DFT-B3LYP
Pyr	222.0	222.4	223.3	214.7	214.3	215.2	7.2	5.8	6.7	5.3[d]	4.3	4.9
2Me-Pyr	226.8	226.5	227.7	219.2	219.5	220.7	8.2	8.8	10.0	6.0[d]	6.5	7.3
3Me-Pyr	225.5	225.6	226.9	217.9	217.8	219.1	7.8	7.0	8.3	5.7[d]	5.1	6.1
4Me-Pyr	226.4	226.5	228.0	218.8	218.9	220.4	8.2	7.4	8.9	6.0[d]	5.4	6.5
2NH_2−Pyr	226.4	226.5	228.0	218.8	219.0	220.5	9.4	9.2	10.7	6.9[e]	6.7	7.9
3NH_2−Pyr	228.1	227.9	229.9	220.5	220.4	222.4	8.2	8.0	10.1	6.0[e]	5.9	7.4
4NH_2−Pyr	234.2	234.7	236.4	226.5	226.9	228.6	12.5	11.8	13.5	9.2[e]	8.7	9.9
2Et-Pyr	227.6	228.6	229.8	220.0	220.6	221.9	8.2	8.2	9.4	6.0[d]	6.0	6.9
3Et-Pyr	226.4	226.6	228.1	218.8	218.9	220.3	7.8	7.3	8.8	5.7[f]	5.4	6.4
4Et-Pyr	227.3	227.1	229.0	219.7	219.0	220.8	8.2	7.6	9.5	6.0[e]	5.6	7.0
2Me-3Me-Pyr	229.2	229.4	230.8	221.6	221.5	223.0	9.0	9.8	11.3	6.6[d]	7.2	8.3
2Me-4Me-Pyr	230.1	230.3	232.0	222.5	222.6	224.2	9.5	9.8	11.5	7.0[d]	7.2	8.4
2Me-5Me-Pyr	229.2	229.3	230.8	221.5	221.7	223.2	8.7	9.0	10.4	6.4[d]	6.6	7.7
2Me-6Me-Pyr	230.2	230.3	231.7	222.5	223.1	224.5	9.1	9.9	11.3	6.7[d]	7.3	8.3
3Me-4Me-Pyr	228.8	229.4	231.1	221.2	221.8	223.4	8.9	8.3	10.0	6.5[d]	6.1	7.3
3Me-5Me-Pyr	228.3	228.6	230.1	220.7	220.7	222.2	8.5	7.6	9.1	6.2[d]	5.6	6.7
2Cl-Pyr	215.3	215.9	216.5	208.0	208.2	208.8	0.7	−1.5	−0.8	0.5[d]	−1.1	−0.6
3Cl-Pyr	215.9	216.8	217.8	208.3	209.1	210.1	3.8	2.5	3.4	2.8[d]	1.8	2.5
4Cl-Pyr	219.0	219.0	220.2	211.3	211.3	212.5	5.2	3.7	4.9	3.8[d]	2.7	3.6
2Cl-4Me-Pyr	220.2	220.0	221.1	212.5	212.3	213.4	2.3	0.2	1.3	1.7[e]	0.1	0.9
2Cl-6Me-Pyr	217.0	219.8	220.7	209.4	212.1	213.0	1.8	0.6	1.5	1.3[e]	0.4	1.1
4CHO-Pyr	216.2	216.4	216.6	208.6	208.8	209.1	6.4	3.4	3.7	4.7[d]	2.5	2.7
MAD		**0.4**	**1.7**		**0.4**	**1.6**		**0.9**	**1.2**		**0.7**	**0.9**
SD		**0.6**	**0.6**		**0.6**	**0.6**		**0.8**	**0.7**		**0.6**	**0.5**
MAX		**2.8**	**3.7**		**2.7**	**3.6**		**3.0**	**2.8**		**2.2**	**2.0**

[a]Experimental gas-phase deprotonation enthalpies and free energies have uncertainties of ∼2 kcal/mol.[158] Experimental pK_as are considered accurate to 0.3 pK_a units. All data presented used a direct calculation scheme (Scheme 1) using 'E2//G2' or 'E7//G2' ΔG^{o}_{g} calculations and 'UA2//Gc5(H2O)' calculations for ΔG^{*}_{S}. See the Computational Methods section for more details and Table 1 for explanation of labels. [b]Reference 158. [c]Derived by converting experimental pK_as using eq 2. [d]Reference 160. [e]Reference 161. [f]Reference 169.

less than the previously mentioned CCSD(T)-F12 MAD. SMD calculations ('E2//G2:SMD2//G2') vary somewhat more (MAD = 5.0 kcal/mol), while CPCM solvation with ROHF electron densities ('E2//G2:UA1//G2') differ substantially more (MAD = 7.4 kcal/mol). ΔG^{*}_{aq} values were calculated assuming a thermodynamically closed cycle (i.e., assuming all pyridinyl and pyridine anions were in the $^2B_1$-like state). In reality this was not always the case, however, and as discussed earlier, the gas-phase references for the anion ΔG^{*}_{S} values sometimes converged to the $^2A_1$-like state. This means that much of the data on the left side of Figure 8a actually involve spurious errors due to thermodynamic inconsistencies.

Figure 8b shows that standard deviations on the whole become smaller when an explicit water is added to the ΔG^{*}_{S} calculation. Here, the microsolvation due to the explicit water molecule permits greater polarization of the pyridine anions, thereby leading to solvation energies correctly referenced to the $^2B_1$-like state in practically all cases. This was found true even for ΔG^{*}_{S} calculations using even more diffuse aVDZ basis sets; however, since the SUAHF radii were parametrized to 6-31+G* calculations, we continue to report solvation energies with the smaller basis set. Indeed, the energy arising from the ΔG^{o}_{g}(bind) used in the implicit/explicit solvation cycle (see Scheme 3) ranged from 2−5 kcal/mol (or 0.1−0.2 eV) depending on the anion, and in most cases this was enough to offset the difference in energy between the $^2A_1$-like and $^2B_1$-like states shown in Figure 7a. The only exceptions to this were the amino-substituted pyridine anions, where the energy differences between the $^2A_1$-like and $^2B_1$-like states were closer to 0.5 eV, and the gas-phase reference energies used in the ΔG^{*}_{S} calculations still remained in the $^2A_1$-like state. Notably, deviations in the DFT-B3LYP calculations using DFT electron densities to calculate ΔG^{*}_{S} now increase compared to Figure 8a, showing that the small deviations in Figure 8a were more likely an artifact of error cancellation.

The most reliable solvation scheme is that which uses both an explicit water as well as geometries optimized under the implicit solvation model. Figure 8c shows all three DFT-based calculations agreeing semiquantitatively with the UCCSD(T)-F12 benchmark calculations. Calculations using ROHF electron densities ('E2//G2:UA1//Gc1(H2O)') still show some spurious deviations (due to overstabilization of the anion due to the wrong reference again being used in the solvation calculation) and therefore are not generally recommended. The deviations in the DFT-B3LYP calculations using UDFT electron densities ('E2//G2:UA2//Gc2(H2O)') in Figure 8c differ from the reference by the same difference that was seen in the gas-phase deprotonation energies shown in Figure 7c, since both this calculation and the benchmark calculation use the same solvation energies. The ensemble of these data also make clear that when ΔG^{*}_{S} values are computed consistently (with the help of explicit water molecules and geometries optimized in solvent), the accuracies of ΔG^{*}_{aq} are affected more by thermodynamic inconsistencies due to using different electronic

Table 3. (Negative of the) Gas-Phase Adiabatic Electron Affinities (-AEAs) of Substituted Pyridines That Form $^2A_1$-like and $^2B_1$-like States of Pyridine Anions (in eV) and Gas-Phase Deprotonation Enthalpies, Deprotonation Free Energies, and Aqueous-Phase Deprotonation Free Energies of Substituted Pyridinyls at T = 298 K (in kcal/mol)[a]

	-(AEA)				ΔH_{gas}				ΔG_{gas}				ΔG^*_{aq}		pK_a	
pyridinyl name	CCSD(T)-F12		DFT-B3LYP		CCSD(T)-F12		DFT-B3LYP		CCSD(T)-F12		DFT-B3LYP		CCSD(T)-F12	DFT-B3LYP	CCSD(T)-F12	DFT-B3LYP
	A1	B1	A1	B1	A1	B1	A1	B1	A1	B1	A1	B1				
Pyr*	0.53	0.71	0.49	0.64	355.0	358.9	355.7	358.7	349.1	353.0	349.8	352.8	39.9	39.6	29.3	29.0
2Me-Pyr*	0.49	0.70	0.48	0.62	354.2	358.6	355.2	358.2	347.8	352.0	348.8	351.7	40.0	39.6	29.3	29.0
3Me-Pyr*	0.54	0.71	0.44	0.67	355.6	359.2	354.6	359.5	348.9	351.8	348.0	352.1	40.5	40.8	29.7	29.9
4Me-Pyr*	0.46	0.78	0.44	0.51	351.6	358.9	352.8	354.4	345.7	351.5	346.9	346.9	41.3	36.7	30.3	26.9
2NH2-Pyr*	0.47	0.94	0.42	0.88	348.1	359.7	347.7	359.0	341.0	351.0	340.6	350.3	41.8	41.1	30.7	30.1
3NH2-Pyr*	0.37	0.87	0.33	0.80	350.6	362.9	350.8	362.5	344.3	354.6	344.5	354.3	45.8	45.5	33.6	33.4
4NH2-Pyr*	0.32	0.66	0.28	0.68	343.7	353.0	343.6	354.4	337.7	343.1	337.6	344.5	40.5	41.8	29.7	30.7
2Et-Pyr*	0.44	0.93	0.38	0.66	353.1	364.9	352.8	359.7	346.3	357.3	346.0	352.0	47.8	42.6	35.1	31.2
3Et-Pyr*	0.38	0.83	0.29	0.53	352.7	362.7	351.8	356.8	346.3	355.7	345.4	349.9	46.5	40.7	34.1	29.9
4Et-Pyr*	0.40	0.79	0.28	0.54	349.6	358.1	348.6	354.0	343.2	351.7	342.2	347.5	43.3	39.2	31.8	28.8
2Me-3Me-Pyr*	0.48	1.02	0.47	0.73	352.2	363.8	353.2	358.6	345.6	357.9	346.7	352.6	49.5	44.2	36.3	32.4
2Me-4Me-Pyr*	0.46	0.81	0.45	0.59	351.5	359.3	352.7	355.5	344.7	352.2	345.8	348.5	43.4	39.6	31.8	29.0
2Me-5Me-Pyr*	0.55	1.01	0.54	0.75	356.0	366.0	357.0	361.2	348.9	359.5	349.9	354.7	46.2	41.4	33.9	30.4
2Me-6Me-Pyr*	0.46	0.69	0.54	0.61	353.5	358.3	356.5	357.6	346.9	351.9	349.9	351.2	40.3	39.6	29.6	29.0
3Me-4Me-Pyr*	0.42	0.86	0.41	0.60	350.4	360.9	351.7	356.2	343.8	353.7	345.1	349.1	45.9	41.2	33.7	30.2
3Me-5Me-Pyr*	0.49	0.72	0.45	0.49	354.7	359.5	355.0	355.5	348.3	352.8	348.5	348.8	41.2	37.2	30.2	27.3
2Cl-Pyr*	--	0.33	--	0.18	--	348.8	--	346.4	--	341.7	--	339.4	30.3	27.9	22.2	20.5
3Cl-Pyr*	--	0.31	--	0.18	--	350.7	--	349.2	--	343.9	--	342.4	33.0	31.5	24.2	23.1
2Cl-4Me-Pyr*	--	0.38	--	0.17	--	348.2	--	344.4	--	341.4	--	337.6	33.1	29.3	24.3	21.5
2Cl-6Me-Pyr*	--	0.40	--	0.22	--	350.3	--	346.9	--	343.0	--	339.6	32.2	28.8	23.6	21.1
4CHO-Pyr*	--	−0.09	--	−0.29	--	335.9	--	334.7	--	328.6	--	327.4	23.6	22.5	17.3	16.5
MAD			**0.05**	**0.17**			**0.9**	**2.8**			**0.9**	**2.8**		**2.8**		**2.0**
SD			**0.04**	**0.09**			**0.7**	**2.0**			**0.7**	**2.0**		**2.0**		**1.4**
MAX			**0.12**	**0.30**			**2.9**	**5.9**			**2.9**	**5.9**		**5.9**		**4.3**

[a]Aqueous pK_as reported in pK_a units. All data presented used a direct calculation scheme (Scheme 1) using 'E2//G2' or 'E7//G2' calculations for ΔG^o_g and 'UA2//Gc5(H2O)' calculations for ΔG^*_s. See the Computational Methods section and Table 1 for more details. Shaded regions denote that the $^2B_1$-like state used in calculations optimized to a transition state with one imaginary frequency. See text for details.

dx.doi.org/10.1021/ct300295g | J. Chem. Theory Comput. 2012, 8, 3187–3206

states in ΔG^*_{aq} calculations rather than accuracies of different solvation models.

SUMMARY

We compiled Table 2 to show our best calculations of substituted pyridinium pK_as and Table 3 to provide our best predictions of substituted pyridinyl pK_as (and related quantities). This study allows us to make several conclusions regarding quantum chemical acidity calculations. First, our analysis of closed shell deprotonations (Figures 2 and 3) shows that a variety of different acidity calculation schemes can produce similarly well-behaved trends when using isodesmic schemes (such as Scheme 4). Nonisodesmic schemes (such as Scheme 1) also perform well as long as error cancellations are optimized, and optimal error cancellation using Scheme 1 for closed shell acidities affords the data in Table 2.

Table 2 shows CCSD(T)-F12 calculated pK_as for substituted pyridinium cations lie between −1.1 (for 2-chloropyridinium) and 8.7 (for 4-aminopyridinium). DFT-B3LYP calculated values are similar, ranging from −0.6 to 9.9. Electron-withdrawing groups such as Cl- or CHO-groups dramatically decrease the gas-phase deprotonation energies and aqueous-phase pK_as for substituted pyridinium molecules, while electron-donating groups such as Me-, NH_2-, and Et- all increase the gas-phase deprotonation energies and aqueous-phase pK_as. Furthermore, the presence of additional Me-groups increases pyridinium pK_as. This trend is expected, since it merely reflects how the substituent affects the stability of the pyridinium cation: the electron-withdrawing groups render the N electron-poor and thus less attractive to the proton (hence the low pK_as) and vice versa for the electron-donating groups.

Our optimized calculation scheme is one way to directly calculate pK_as for substituted pyridinium cations with quantitative accuracy. Overall, it reproduces qualitative and quantitative trends in gas-phase deprotonation enthalpies and free energies with MADs of ∼0.4 kcal/mol (for CCSD(T)-F12 calculations) or ∼1.7 kcal/mol (for DFT-B3LYP calculations) and SDs of ∼0.6 kcal/mol for both sets of energies. Notably, DFT-B3LYP energies are always overestimated. When CCSD(T)-F12 calculations are too computationally demanding, this study shows that standard KSDFT with the B3LYP functional is capable of obtaining chemical accuracy even though gas-phase deprotonation free energies are very large − from 208.6 kcal/mol (for **4CHO-Pyr**) to 226.5 kcal/mol (for **4NH$_2$-Pyr**). The largest errors found in gas-phase energies occur with **2Cl-6Me-Pyr** (∼3.7 kcal/mol), but since this is the lone species with an error larger than 2 kcal/mol (found by both CCSD(T)-F12 and DFT-B3LYP), we conclude that the experimental value for this deprotonation may need to be re-evaluated.

Using these DFT-B3LYP ΔG°_g values in thermodynamic cycles for ΔG^*_{aq} results in MADs of only 1.2 kcal/mol and a SD of 0.7 kcal/mol, while CCSD(T)-F12 MADs are slightly lower (0.9 kcal/mol) and the SD is slightly higher (0.8 kcal/mol). These final results were obtained using an implicit solvation model with one explicit water molecule. Pyridinium acidities with electron-donating groups were slightly overestimated, while pyridinium acidities with electron-withdrawing groups were slightly underestimated. The largest error in ΔG^*_{aq} occurred for **4CHO-Pyr**, where the error of 2.8 kcal/mol corresponds to an error of 2.0 in pK_a units with DFT-B3LYP (and errors of 3.0 kcal/mol and 2.2 pK_a units using CCSD(T)-F12 calculations).

Regarding the data in Table 3, one sees that pK_as for substituted pyridinyl molecules are significantly higher than their corresponding pyridinium parents, meaning they are much less likely to deprotonate under electrochemical conditions. Here the predicted pK_as range from ∼17 (for **4CHO-Pyr**) to as high as ∼35 (for **2Me-3Me-Pyr**). To understand these pK_as, we revisit the earlier discussion on gas-phase energies. Since pyridinyl deprotonations produce an anion, electron repulsion plays a larger role in determining its acidity constant. Normally, one would expect that electron-donating groups destabilize the radical anion, resulting in larger deprotonation energies. However, when large enough basis sets are used, the electron repulsion within the pyridinyl leads to molecules with broken symmetry (the $^2A_1$-like states), and now substituents *stabilize* the pyridine anions (by allowing more charge delocalization). This in turn causes the deprotonation energies of substituted pyridinyls to appear to be less than those from the nonsubstituted pyridinyl. Whether or not these are valid deprotonation energies, calculating the radical pK_as requires characterizing the higher energy π antibonding $^2B_1$-like states in order to obtain thermodynamically consistent solvation calculations. Note that we consistently find $^2B_1$ ground states for these species when they are solvated, so it is critical to calculate the corresponding gas-phase $^2B_1$ state to complete the cycle. Since experimental data are not presently available for ΔG°_g or ΔG^*_{aq} values, it is difficult to know the overall accuracies of the pyridinyl deprotonation energies (and it would likewise be difficult to identify whether the formed pyridine anion was in the $^2A_1$-like or $^2B_1$-like state). This in turn makes pyridinyl acidities challenging to ascertain, however by consistently keeping track of the different anion radical states used in solvation cycles, pK_as of several different calculations agree with benchmark calculations to within ∼4 pK_a units, and this is mainly due to the need for higher levels of correlation to adequately characterize $^2B_1$-like states.

As with the pyridinium molecules of Table 1, data indicate that electron-withdrawing groups such as Cl- and CHO- always decrease pK_as compared to the other substituents. Although results in Table 3 have some uncertainties, the conclusion reached upon comparing the relative acidities of pyridinium versus pyridinyl is entirely unambiguous: the acidity constants of substituted pyridinyl species are between 10 to 20 pK_a units higher than their pyridinium counterparts, and therefore they are highly unlikely to play any role in acid/base chemistry under electrocatalytic conditions.

CONCLUDING REMARKS

We have used computational quantum chemistry to benchmark and validate calculated acidity constants for differently substituted pyridinium and pyridinyl species. In general, when pK_as are calculated from Scheme 4 and referenced to an empirical pK_a value, almost all solvation models perform similarly well for closed shell deprotonations. In order to predict absolute pK_as without the empirical pK_a value, we calculated pK_as using Scheme 1. After accounting for the different user-defined parameters needed for solvation calculations, the best combination of parameters (using the CPCM-SUAHF solvation model with one explicit water, DFT-B3LYP/6-31+G* electron densities to solve for the electrostatic potential, while omitting nonelectrostatic energy contributions) resulted in a calculation scheme that reproduced 22 known pK_as to within 0.9 pK_a units. These data compared well to a similar scheme using even more robust electronic energies

calculated from explicitly correlated CCSD(T)-F12 calculations. We then used this same scheme to predict pK_as for the corresponding pyridinyl radicals, which are significantly less well-behaved partly due to symmetry breaking in some radical anion species. Radical solvation energies are likewise difficult to assess (also with no available experimental comparison) and are much more sensitive to how the solvation energies were obtained. Including an explicit water molecule in solvation calculations is highly recommended as this helps stabilize the radical anion valence state that is needed for a thermodynamically consistent acidity calculation. Our calculations find pyridinyl acidities ranging from 16.5 (for the most-acidic 4-formyl pyridinyl species) up to ∼35 (for the 2-ethyl pyridinyl species). Based on comparisons between different calculation models, we believe our radical acidity constants are conservatively accurate to within 5 pK_a units (not including additional uncertainties due to the empirical proton solvation energy employed). The unsubstituted parent pyridinyl radical has a predicted pK_a of 29, which means that pyridinyl species should never be considered acidic at all, and their aqueous-phase deprotonations can be excluded from homogeneous photoelectrochemical reaction mechanisms.

■ ASSOCIATED CONTENT

Ⓢ Supporting Information

Additional figures (S1−S6) reporting data referred to in the text. This material is available free of charge via the Internet at http://pubs.acs.org.

■ AUTHOR INFORMATION

Corresponding Author

*E-mail: eac@princeton.edu.

Notes

The authors declare no competing financial interest.

■ ACKNOWLEDGMENTS

J.A.K. thanks Prof. Kirk Peterson for his help running the Molpro code. We thank Dr. Michele Pavone and Andrew Ritzmann for helpful discussions, and Prof. Andrew Bocarsly for helpful discussions and for recommending that we pursue computational schemes to determine pK_as for pyridinyl species. This work was funded by the Air Force Office of Scientific Research through the MURI program under AFOSR Award No. FA9550-10-1-057.

■ REFERENCES

(1) Kruger, P. *Alternative Energy Resources: The Quest for Sustainable Energy*;,1st ed.; John Wiley & Sons, Inc.: Hoboken, NJ, 2006.

(2) Moselle, B.; Padilla, J.; Schmalensee, R. *Harnessing Renewable Energy in Electric Power Systems: Theory, Practice, Policy*; RFF Press: Washington, DC, 2010.

(3) Olah, G. A.; Goeppert, A.; Prakash, G. K. S. *Beyond Oil and Gas: The Methanol Economy*, 1st ed.; Wiley-VCH: Weinheim, 2006.

(4) Cook, T. R.; Dogutan, D. K.; Reece, S. Y.; Surendranath, Y.; Teets, T. S.; Nocera, D. G. *Chem. Rev.* **2010**, *110*, 6474−6502.

(5) Hains, A. W.; Liang, Z.; Woodhouse, M. A.; Gregg, B. A. *Chem. Rev.* **2010**, *110*, 6689−6735.

(6) Hochbaum, A. I.; Yang, P. *Chem. Rev.* **2010**, *110*, 527−546.

(7) McEvoy, J. P.; Brudvig, G. W. *Chem. Rev.* **2006**, *106*, 4455−4483.

(8) Navarro, R. M.; Alvarez-Galván, M. C.; Villoria de la Mano, J. A.; Al-Zahrani, S. M.; Fierro, J. L. G. *Energy Environ. Sci.* **2010**, *3*, 1865−1882.

(9) Walter, M. G.; Warren, E. L.; McKone, J. R.; Boettcher, S. W.; Mi, Q.; Santori, E. A.; Lewis, N. S. *Chem. Rev.* **2010**, *110*, 6446−6473.

(10) Benson, E. E.; Kubiak, C. P.; Sathrum, A. J.; Smieja, J. M. *Chem. Soc. Rev.* **2009**, *38*, 89−99.

(11) Morris, A. J.; Meyer, G. J.; Fujita, E. *Acc. Chem. Res.* **2009**, *42*, 1983−1994.

(12) Olah, G. A.; Prakash, G. K. S.; Goeppert, A. *J. Am. Chem. Soc.* **2011**, *133*, 12881−12898.

(13) Tomasi, J.; Mennucci, B.; Cammi, R. *Chem. Rev.* **2005**, *105*, 2999−3094.

(14) Tomasi, J.; Persico, M. *Chem. Rev.* **1994**, *94*, 2027−2094.

(15) Cramer, C. J.; Truhlar, D. G. *Chem. Rev.* **1999**, *99*, 2161−2200.

(16) Ahlquist, M. S. G. *J. Mol. Catal. A: Chem.* **2010**, *324*, 3−8.

(17) Anderson, B. J.; Keith, J. A.; Sigman, M. S. *J. Am. Chem. Soc.* **2010**, *132*, 11872−11874.

(18) Comas-Vives, A.; González-Arellano, C.; Corma, A.; Iglesias, M.; Sánchez, F.; Ujaque, G. *J. Am. Chem. Soc.* **2006**, *128*, 4756−4765.

(19) Decharin, N.; Popp, B. V.; Stahl, S. S. *J. Am. Chem. Soc.* **2011**, *133*, 13268−13271.

(20) Goddard, W. A., III; Liu, L.; Mueller, J. E.; Pudar, S.; Nielsen, R. J. *Top. Catal.* **2011**, *54*, 659−668.

(21) Jinnouchi, R.; Anderson, A. B. *Phys. Rev. B* **2008**, *77*, 245417.

(22) Liu, C.; Cundari, T. R.; Wilson, A. K. *Inorg. Chem.* **2011**, *50*, 8782−8789.

(23) Sánchez, V. M.; de la Llave, E.; Scherlis, D. A. *Langmuir* **2011**, *27*, 2411−2419.

(24) Sha, Y.; Yu, T. H.; Liu, Y.; Merinov, B. V.; Goddard, W. A., III *J. Phys. Chem. Lett.* **2010**, *1*, 856−861.

(25) Wang, H.-F.; Liu, Z.-P. *J. Phys. Chem. C* **2009**, *113*, 17502−17508.

(26) Adam, K. R. *J. Phys. Chem. A* **2002**, *106*, 11963−11972.

(27) Bryantsev, V. S.; Diallo, M. S.; Goddard, W. A., III *J. Phys. Chem. A* **2007**, *111*, 4422−4430.

(28) Burger, S. K.; Liu, S.; Ayers, P. W. *J. Phys. Chem. A* **2011**, *115*, 1293−1304.

(29) Caballero, N. A.; Melendez, F. J.; Muñoz-Caro, C.; Niño, A. *Biophys. Chem.* **2006**, *124*, 155−160.

(30) Camaioni, D. M.; Dupuis, M.; Bentley, J. *J. Phys. Chem. A* **2003**, *107*, 5778−5788.

(31) Casasnovas, R.; Frau, J.; Ortega-Castro, J.; Salvà, A.; Donoso, J.; Muñoz, F. *J. Mol. Struct.: THEOCHEM* **2009**, *912*, 5−12.

(32) Chen, I.-J.; MacKerell, A. D., Jr. *Theor. Chem. Acc.* **2000**, *103*, 483−494.

(33) Chipman, D. M. *J. Phys. Chem. A* **2002**, *106*, 7413−7422.

(34) Eckert, F.; Diedenhofen, M.; Klamt, A. *Mol. Phys.* **2010**, *108*, 229−241.

(35) Fu, Y.; Liu, L.; Li, R.-Q.; Liu, R.; Guo, Q.-X. *J. Am. Chem. Soc.* **2004**, *126*, 814−822.

(36) Glasovac, Z.; Eckert-Maksić, M.; Maksić, Z. B. *New J. Chem.* **2009**, *33*, 588.

(37) Ho, J.; Coote, M. L.; Franco-Pérez, M.; Gómez-Balderas, R. *J. Phys. Chem. A* **2010**, *114*, 11992−12003.

(38) Jacquemin, D.; Perpete, E. A.; Ciofini, I.; Adamo, C. *J. Phys. Chem. A* **2008**, *112*, 794−796.

(39) Kelly, C. P.; Cramer, C. J.; Truhlar, D. G. *J. Phys. Chem. A* **2006**, *110*, 2493−2499.

(40) Klicić, J. J.; Friesner, R. A.; Liu, S.-Y.; Guida, W. C. *J. Phys. Chem. A* **2002**, *106*, 1327−1335.

(41) Liptak, M. D.; Gross, K. C.; Seybold, P. G.; Feldgus, S.; Shields, G. C. *J. Am. Chem. Soc.* **2002**, *124*, 6421−6427.

(42) Lee, I.; Kim, C. K.; Han, I. S.; Lee, H. W.; Kim, W. K.; Kim, Y. B. *J. Phys. Chem. B* **1999**, *103*, 7302−7307.

(43) Makowski, M.; Sadowski, R.; Augustin-Nowacka, D.; Chmurzyński, L. *J. Phys. Chem. A* **2001**, *105*, 6743−6749.

(44) Pliego, J. R.; Riveros, J. M. *J. Phys. Chem. A* **2002**, *106*, 7434−7439.

(45) Saracino, G. A. A.; Improta, R.; Barone, V. *Chem. Phys. Lett.* **2003**, *373*, 411−415.

(46) Takano, Y.; Houk, K. N. *J. Chem. Theory Comput.* **2005**, *1*, 70−77.

(47) Verdolino, V.; Cammi, R.; Munk, B. H.; Schlegel, H. B. *J. Phys. Chem. B* **2008**, *112*, 16860−16873.
(48) Zhang, S.; Baker, J.; Pulay, P. *J. Phys. Chem. A* **2010**, *114*, 432−442.
(49) Sviatenko, L.; Isayev, O.; Gorb, L.; Hill, F.; Leszczynski, J. *J. Comput. Chem.* **2011**, *32*, 2195−2203.
(50) Ali, S. T.; Karamat, S.; Kóňa, J.; Fabian, W. M. F. *J. Phys. Chem. A* **2010**, *114*, 12470−12478.
(51) Ho, J.; Coote, M. L. *Wiley Interdiscip. Rev.: Comput. Mol. Sci.* **2011**, *1*, 649−660.
(52) Ho, J.; Coote, M. L. *Theor. Chem. Acc.* **2009**, *125*, 3−21.
(53) Hill, M. D. *Chem.—Eur. J.* **2010**, *16*, 12052−12062.
(54) Hanson, S. K.; Baker, R. T.; Gordon, J. C.; Scott, B. L.; Kibler, L. A.; Thorn, D. L. *J. Am. Chem. Soc.* **2010**, *132*, 17804−17816.
(55) Foster, J. W.; Moat, A. G. *Microbiol. Rev.* **1980**, *44*, 83−105.
(56) Martoprawiro, M.; Bacskay, G. *Mol. Phys.* **1995**, *85*, 573−585.
(57) Dkhissi, A.; Adamowicz, L.; Maes, G. *J. Phys. Chem. A* **2000**, *104*, 2112−2119.
(58) Schlücker, S.; Singh, R. K.; Asthana, B. P.; Popp, J.; Kiefer, W. *J. Phys. Chem. A* **2001**, *105*, 9983−9989.
(59) Mason, P. E.; Neilson, G. W.; Dempsey, C. E.; Price, D. L.; Saboungi, M.-L.; Brady, J. W. *J. Phys. Chem. B* **2010**, *114*, 5412−5419.
(60) Marczak, W.; Czech, B.; Almásy, L.; Lairez, D. *Phys. Chem. Chem. Phys.* **2011**, *13*, 6260−6269.
(61) Wolken, J. K.; Tureček, F. *J. Am. Chem. Soc.* **1999**, *121*, 6010−6018.
(62) Moiroux, J.; Deycard, S.; Malinski, T. *J. Electroanal. Chem.* **1985**, *194*, 99−108.
(63) Seshadri, G.; Lin, C.; Bocarsly, A. B. *J. Electroanal. Chem.* **1994**, *372*, 145−150.
(64) Barton, E. E.; Rampulla, D. M.; Bocarsly, A. B. *J. Am. Chem. Soc.* **2008**, *130*, 6342−6344.
(65) Barton Cole, E.; Lakkaraju, P. S.; Rampulla, D. M.; Morris, A. J.; Abelev, E.; Bocarsly, A. B. *J. Am. Chem. Soc.* **2010**, *132*, 11539−11551.
(66) Morris, A. J.; McGibbon, R. T.; Bocarsly, A. B. *ChemSusChem* **2011**, *4*, 191−196.
(67) Keith, J. A.; Carter, E. A. *J. Am. Chem. Soc.* **2012**, *134*, 7580−7583.
(68) Ögretir, C.; Özögüt, D.; Yarligan, S.; Arslan, T. *J. Mol. Struct.; THEOCHEM* **2006**, *759*, 73−78.
(69) Güven, A. *Int. J. Mol. Sci.* **1995**, *6*, 257−275.
(70) Hawe, G. I.; Alkorta, I.; Popelier, P. L. A. *J. Chem. Inf. Model.* **2010**, *50*, 87−96.
(71) Yu, A.; Liu, Y.; Wang, Y. *Chem. Phys. Lett.* **2007**, *436*, 276−279.
(72) Naumov, S.; von Sonntag, C. *J. Phys. Org. Chem.* **2011**, *24*, 600−602.
(73) Mangold, M.; Rolland, L.; Costanzo, F.; Sprik, M.; Sulpizi, M.; Blumberger, J. *J. Chem. Theory Comput.* **2011**, *7*, 1951−1961.
(74) Zhu, X.-Q.; Wang, C.-H.; Liang, H. *J. Org. Chem.* **2010**, *75*, 7240−7257.
(75) McDonald, W. J.; Einarsdóttir, Ó. *J. Phys. Chem. B* **2010**, *114*, 6409−6425.
(76) Adhikary, A.; Kumar, A.; Khanduri, D.; Sevilla, M. D. *J. Am. Chem. Soc.* **2008**, *130*, 10282−10292.
(77) Burgett, R. A.; Bao, X.; Villamena, F. A. *J. Phys. Chem. A* **2008**, *112*, 2447−2455.
(78) Armstrong, D. A.; Waltz, W. L.; Rauk, A. *Can. J. Chem.* **2006**, *84*, 1614−1619.
(79) Georgieva, M. K.; Velcheva, E. A. *Int. J. Quantum Chem.* **2006**, *106*, 1316−1322.
(80) Villamena, F. A.; Merle, J. K.; Hadad, C. M.; Zweier, J. L. *J. Phys. Chem. A* **2005**, *109*, 6083−6088.
(81) Chen, X.; Syrstad, E. A.; Nguyen, M. T.; Gerbaux, P.; Tureček, F. *J. Phys. Chem. A* **2004**, *108*, 9283−9293.
(82) Nenner, I.; Schulz, G. J. *J. Chem. Phys.* **1975**, *62*, 1747−1758.
(83) Simons, J. *J. Phys. Chem. A* **2008**, *112*, 6401−6511.
(84) Simons, J.; Jordan, K. D. *Chem. Rev.* **1987**, *87*, 535−555.
(85) Kosower, E. M.; Teuerstein, A.; Burrows, H. D.; Swallow, A. J. *J. Am. Chem. Soc.* **1978**, *100*, 5185−5190.
(86) Gębicki, J.; Marcinek, A.; Zielonka, J. *Acc. Chem. Res.* **2004**, *37*, 379−386.
(87) Brühlmann, U.; Hayon, E. *J. Am. Chem. Soc.* **1974**, *96*, 6169−6175.
(88) Neta, P. *Radiat. Res.* **1972**, *52*, 471−480.
(89) Neta, P.; Patterson, L. K. *J. Phys. Chem.* **1974**, *78*, 2211−2217.
(90) Ben-Naim, A. *J. Phys. Chem.* **1978**, *82*, 792−803.
(91) Ben-Naim, A.; Marcus, Y. *J. Chem. Phys.* **1984**, *81*, 2016−2027.
(92) Ho, J.; Klamt, A.; Coote, M. L. *J. Phys. Chem. A* **2010**, *114*, 13442−13444.
(93) Asthagiri, D.; Pratt, L. R.; Ashbaugh, H. S. *J. Chem. Phys.* **2003**, *119*, 2702−2708.
(94) Asthagiri, D.; Pratt, L. R.; Paulaitis, M. E.; Rempe, S. B. *J. Am. Chem. Soc.* **2004**, *126*, 1285−1289.
(95) Tawa, G. J.; Topol, I. A.; Burt, S. K.; Caldwell, R. A.; Rashin, A. A. *J. Chem. Phys.* **1998**, *109*, 4852−4863.
(96) Mejías, J. A.; Lago, S. *J. Chem. Phys.* **2000**, *113*, 7306−7316.
(97) Zhan, C.-G.; Dixon, D. A. *J. Phys. Chem. A* **2001**, *105*, 11534−11540.
(98) Zhan, C.-G.; Dixon, D. A. *J. Phys. Chem. A* **2002**, *106*, 9737−9744.
(99) Zhan, C.-G.; Dixon, D. A. *J. Phys. Chem. A* **2004**, *108*, 2020−2029.
(100) Bryantsev, V. S.; Diallo, M. S.; Goddard, W. A., III *J. Phys. Chem. B* **2008**, *112*, 9709−9719.
(101) Pliego, J. R.; Riveros, J. M. *J. Phys. Chem. A* **2001**, *105*, 7241−7247.
(102) Marx, D. *ChemPhysChem* **2006**, *7*, 1848−1870.
(103) Stoyanov, E. S.; Stoyanova, I. V.; Reed, C. A. *J. Am. Chem. Soc.* **2010**, *132*, 1484−1485.
(104) Tissandier, M. D.; Cowen, K. A.; Feng, W. Y.; Gundlach, E.; Cohen, M. H.; Earhart, A. D.; Coe, J. V.; Tuttle, T. R. *J. Phys. Chem. A* **1998**, *102*, 7787−7794.
(105) Kelly, C. P.; Cramer, C. J.; Truhlar, D. G. *J. Phys. Chem. B* **2006**, *110*, 16066−16081.
(106) Camaioni, D. M.; Schwerdtfeger, C. A. *J. Phys. Chem. A* **2005**, *109*, 10795−10797.
(107) Pauling, L. *The Nature of the Chemical Bond and the Structure of Molecules and Crystals; An Introduction to Modern Structural Chemistry*, 3rd ed.; Cornell University Press: Ithaca, 1960.
(108) Bondi, A. *J. Phys. Chem.* **1964**, *68*, 441−451.
(109) Barone, V.; Cossi, M.; Tomasi, J. *J. Chem. Phys.* **1997**, *107*, 3210−3221.
(110) Nicholls, A.; Honig, B. *J. Comput. Chem.* **1991**, *12*, 435−445.
(111) Marten, B.; Kim, K.; Cortis, C.; Friesner, R. A.; Murphy, R. B.; Ringnalda, M. N.; Sitkoff, D.; Honig, B. *J. Phys. Chem.* **1996**, *100*, 11775−11788.
(112) Tannor, D. J.; Marten, B.; Murphy, R.; Friesner, R. A.; Sitkoff, D.; Nicholls, A.; Honig, B.; Ringnalda, M.; Goddard, W. A., III *J. Am. Chem. Soc.* **1994**, *116*, 11875−11882.
(113) Baker, N. A.; Sept, D.; Joseph, S.; Holst, M. J.; McCammon, J. A. *Proc. Natl. Acad. Sci.* **2001**, *98*, 10037−10041.
(114) Cancès, E.; Mennucci, B.; Tomasi, J. *J. Chem. Phys.* **1997**, *107*, 3032−3041.
(115) Chipman, D. M. *J. Chem. Phys.* **2000**, *112*, 5558−5565.
(116) Klamt, A. *J. Phys. Chem.* **1995**, *99*, 2224−2235.
(117) Klamt, A.; Schüürmann, G. *J. Chem. Soc., Perkin Trans. 2* **1993**, 799−805.
(118) Barone, V.; Cossi, M. *J. Phys. Chem. A* **1998**, *102*, 1995−2001.
(119) Marenich, A. V.; Cramer, C. J.; Truhlar, D. G. *J. Phys. Chem. B* **2009**, *113*, 6378−6396.
(120) Cramer, C. J.; Truhlar, D. G. *Acc. Chem. Res.* **2008**, *41*, 760−768.
(121) Klamt, A.; Mennucci, B.; Tomasi, J.; Barone, V.; Curutchet, C.; Orozco, M.; Luque, F. J. *Acc. Chem. Res.* **2009**, *42*, 489−492.
(122) Gordon, M. S.; Schmidt, M. W. In *Theory and Applications of Computational Chemistry: The First Forty Years*; Dykstra, C., Frenking, G., Kim, K., Scuseria, G., Eds.; Elsevier Science: Amsterdam, 2005; pp 1167−1189.

(123) Schmidt, M. W.; Baldridge, K. K.; Boatz, J. A.; Elbert, S. T.; Gordon, M. S.; Jensen, J. H.; Koseki, S.; Matsunaga, N.; Nguyen, K. A.; Su, S.; Windus, T. L.; Dupuis, M.; Montgomery, J. A., Jr *J. Comput. Chem.* **1993**, *14*, 1347−1363.
(124) Roothaan, C. C. J. *Rev. Mod. Phys.* **1960**, *32*, 179−185.
(125) Pople, J.; Nesbet, R. *J. Chem. Phys.* **1954**, *22*, 571−572.
(126) Becke, A. D. *Phys. Rev. A* **1988**, *38*, 3098−3100.
(127) Lee, C.; Yang, W.; Parr, R. G. *Phys. Rev. B* **1988**, *37*, 785−789.
(128) Vosko, S. H.; Wilk, L.; Nusair, M. *Can. J. Phys.* **1980**, *58*, 1200−1211.
(129) Hariharan, P. C.; Pople, J. A. *Theor. Chim. Acta* **1973**, *28*, 213−222.
(130) Dunning, T. H. *J. Chem. Phys.* **1989**, *90*, 1007−1023.
(131) Knizia, G.; Adler, T. B.; Werner, H.-J. *J. Chem. Phys.* **2009**, *130*, 054104.
(132) Werner, H.-J.; Knowles, P. J.; Knizia, G.; Manby, F. R.; Schütz, M.; Celani, P.; Korona, T.; Lindh, R.; Mitrushenkov, A.; Rauhut, G.; Shamasundar, K. R.; Adler, T. B.; Amos, R. D.; Bernhardsson, A.; Berning, A.; Cooper, D. L.; Deegan, M. J. O.; Dobbyn, A. J.; Eckert, F.; Goll, E.; Hampel, C.; Hesselmann, A.; Hetzer, G.; Hrenar, T.; Jansen, G.; Köppl, C.; Liu, Y.; Lloyd, A. W.; Mata, R. A.; May, A. J.; McNicholas, S. J.; Meyer, W.; Mura, M. E.; Nicklass, A.; O'Neill, D. P.; Palmieri, P.; Pflüger, K.; Pitzer, R.; Reiher, M.; Shiozaki, T.; Stoll, H.; Stone, A. J.; Tarroni, R.; Thorsteinsson, T.; Wang, M.; Wolf, A. *MOLPRO, version 2010.1, a package of ab initio programs; molpro* **2010**.
(133) Weigend, F. *Phys. Chem. Chem. Phys.* **2002**, *4*, 4285−4291.
(134) Weigend, F.; Köhn, A.; Hättig, C. *J. Chem. Phys.* **2002**, *116*, 3175−3183.
(135) Yousaf, K. E.; Peterson, K. A. *Chem. Phys. Lett.* **2009**, *476*, 303−307.
(136) Cramer, C. J. *Essentials of Computational Chemistry: Theories and Models*, 2nd ed.; John Wiley & Sons, Inc.: Hoboken, NJ, 2004.
(137) Johnson, R. D., III NIST Computational Chemistry Comparison and Benchmark Database NIST Standard Reference Database Number 101 Release 15b, August 2011, Johnson, R. D., III, Ed.; 2011.
(138) Sommerfeld, T.; Weber, R. J. *J. Phys. Chem. A* **2011**, *115*, 6675−6682.
(139) Puiatti, M.; Vera, D. M. A.; Pierini, A. B. *Phys. Chem. Chem. Phys.* **2009**, *11*, 9013−9024.
(140) Peach, M. J. G.; De Proft, F.; Tozer, D. J. *J. Phys. Chem. Lett.* **2010**, *1*, 2826−2831.
(141) *Jaguar*; Schrödinger, LLC: New York, NY, 2007.
(142) Curtiss, L. A.; Raghavachari, K.; Redfern, P. C.; Rassolov, V.; Pople, J. A. *J. Chem. Phys.* **1998**, *109*, 7764−7776.
(143) Curtiss, L. A.; Redfern, P. C.; Raghavachari, K. *J. Chem. Phys.* **2007**, *127*, 124105.
(144) Curtiss, L. A.; Redfern, P. C.; Raghavachari, K. *J. Chem. Phys.* **2007**, *126*, 084108.
(145) Curtiss, L. A.; Redfern, P. C.; Raghavachari, K.; Rassolov, V.; Pople, J. A. *J. Chem. Phys.* **1999**, *110*, 4703−4709.
(146) Boese, A. D.; Oren, M.; Atasoylu, O.; Martin, J. M. L.; Kállay, M.; Gauss, J. *J. Chem. Phys.* **2004**, *120*, 4129−4141.
(147) Martin, J. M. L.; de Oliveira, G. *J. Chem. Phys.* **1999**, *111*, 1843−1856.
(148) Montgomery, J. A.; Frisch, M. J.; Ochterski, J. W.; Petersson, G. A. *J. Chem. Phys.* **1999**, *110*, 2822−2827.
(149) Montgomery, J. A.; Frisch, M. J.; Ochterski, J. W.; Petersson, G. A. *J. Chem. Phys.* **2000**, *112*, 6532−6542.
(150) Montgomery, J. A.; Ochterski, J. W.; Petersson, G. A. *J. Chem. Phys.* **1994**, *101*, 5900−5909.
(151) Ochterski, J. W.; Petersson, G. A.; Montgomery, J. A. *J. Chem. Phys.* **1996**, *104*, 2598−2619.
(152) Petersson, G. A.; Bennett, A.; Tensfeldt, T. G.; Al-Laham, M. A.; Shirley, W. A.; Mantzaris, J. *J. Chem. Phys.* **1988**, *89*, 2193−2218.
(153) Liptak, M. D.; Shields, G. C. *J. Am. Chem. Soc.* **2001**, *123*, 7314−7319.
(154) Ho, J.; Coote, M. L. *J. Chem. Theory Comput.* **2009**, *5*, 295−306.
(155) Moser, A.; Range, K.; York, D. M. *J. Phys. Chem. B* **2010**, *114*, 13911−13921.
(156) Jang, Y. H.; Goddard, W. A., III; Noyes, K. T.; Sowers, L. C.; Hwang, S.; Chung, D. S. *J. Phys. Chem. B* **2003**, *107*, 344−357.
(157) Rogstad, K. N.; Jang, Y. H.; Sowers, L. C.; Goddard, W. A., III *Chem. Res. Toxicol.* **2003**, *16*, 1455−1462.
(158) Hunter, E. P. L.; Lias, S. G. *J. Phys. Chem. Ref. Data* **1998**, *27*, 413−656.
(159) McQuarrie, D. A. *Statistical Mechanics*, 1st ed.; University Science Books: Sausalito, 2000.
(160) In *CRC Handbook of Chemistry and Physics*; Haynes, W. M., Ed.; CRC Press/Taylor and Francis: Boca Raton, 2011.
(161) ChemicalBook Inc. ChemicalBook. http://www.chemicalbook.com/ (accessed July 2012).
(162) Koort, E.; Herodes, K.; Pihl, V.; Leito, I. *Anal. Bioanal. Chem.* **2004**, *379*, 720−729.
(163) Wong, M. W.; Radom, L. *J. Phys. Chem.* **1995**, *99*, 8582−8588.
(164) Chempath, S.; Pratt, L. R.; Paulaitis, M. E. *J. Chem. Phys.* **2009**, *130*, 054113.
(165) da Silva, E. F.; Svendsen, H. F.; Merz, K. M. *J. Phys. Chem. A* **2009**, *113*, 6404−6409.
(166) Aquilante, F.; De Vico, L.; Ferré, N.; Ghigo, G.; Malmqvist, P.-Å; Neogrády, P.; Pedersen, T. B.; Pitoňák, M.; Reiher, M.; Roos, B. O.; Serrano-Andrés, L.; Urban, M.; Veryazov, V.; Lindh, R. *J. Comput. Chem.* **2010**, *31*, 224−247.
(167) Jensen, F. *J. Chem. Theory Comput.* **2010**, *6*, 2726−2735.
(168) Private communication with Prof. Andrew B. Bocarsly.
(169) Tenenbaum, L. E. In *The Chemistry of Heterocyclic Compounds, Pyridine and Its Derivatives*; Klingsberg, E., Ed.; John Wiley & Sons: New York, 1961; Vol. *14/2*, p 176.